DESIGN AND EVALUATION OF A SMALL-SCALE PORTABLE HYBRID ROCKET ENGINE TEST STAND

By

TANNER PRICE

Bachelor of Science in Aerospace Engineering
Oklahoma State University
Stillwater, Oklahoma
2021

Bachelor of Science in Mechanical Engineering
Oklahoma State University
Stillwater, Oklahoma
2021

Submitted to the Faculty of the
Graduate College of the
Oklahoma State University
in partial fulfillment of
the requirements for
the Degree of
MASTER OF SCIENCE
May, 2023

DESIGN AND EVALUATION OF A SMALL-SCALE PORTABLE HYBRID ROCKET ENGINE TEST STAND

Thesis Approved:

Dr. Kurt Rouser

Thesis Advisor

Dr. Khaled Sallam

Dr. Rob Agnew

ACKNOWLEDGMENTS

I would like to thank my advisor Dr. Rouser for his his guidance and encouragement throughout the course of this study. I would also like to thank my committee members Dr. Sallam and Dr. Agnew for their insight and advice for this study. Additionally, I would like to thank the amazing graduate and undergraduate researchers of the Oklahoma State University Richmond Hill Research Laboratory, both past and present, especially Daniel Velasco, Joshua Johnsen, Haden Glasgow, Zac Bycko, and Chris Rathman for their willingness to provide assistance and guidance over the course of this study and my graduate experience.

I would like to thank my parents for their help, encouragement, and patience with me in the pursuit of my dreams. Your unending support has helped me to get where I am today and none of this would have been possible without you. Finally, I would like to thank my wife, Julia, for pushing me to be the best version of myself and always reminding me to enjoy life.

Acknowledgments reflect the views of the author and are not endorsed by committee members or Oklahoma State University.

Name: TANNER PRICE

Date of Degree: MAY, 2023

Title of Study: DESIGN AND EVALUATION OF A SMALL-SCALE PORTABLE HYBRID ROCKET ENGINE TEST STAND

Major Field: MECHANICAL AND AEROSPACE ENGINEERING

Abstract: This paper presents the design and evaluation of a small, portable hybrid rocket test stand that can accommodate up to a 3-in diameter engine casing. The primary goal of this study is to determine the most effective way to build a hybrid rocket test stand for fundamental research purposes. Various design ideas were considered, including the use of roller bearings and a vertically oriented test stand. The final design of the stand is oriented horizontally with the use of 3 flat aluminum plates mounted to linear bearings on T-slot structural framing. The linear bearings allow the most forward aluminum plate to contact and press against the load cell while maintaining minimal friction with the T-slot structural framing. The oxidizer delivery system begins at a 10-lb NOS bottle at 775-psi, going through an adjustable pressure regulator, through an on/off solenoid valve, and finally through an orifice plate before being injected into the combustion chamber. The test stand uses a Futek LLB400 button load cell with a 500-lb capacity, to measure the thrust produced by the engine. A LabVIEW Virtual Instrument controls the solenoid valve, the ignition process, and thrust measurement. Thrust and impulse evaluations of the hybrid rocket engine were conducted on a 1.5-in diameter solid fuel grain over various mass flow rates controlled by the pressure regulator at 200, 300, and 400-psi, the open area of the orifice plate at 0.24-in, and nozzle throat diameters at 13/64-in, 16/64-in, 19/64-in and 25/64-in. All solid fuel grains were composed of 3D printed Polylactic Acid and had a typical Bates grain geometry with a core size of 0.65-in, length of 3.5-in, and 50% infill. The constructed test stand showed an optimal range of nozzle sizes between the #16 and #19 nozzles. The stand also demonstrated the ability to resolve differences in thrust and impulse at a 90% confidence level; showing the design of the test stand is viable for future research purposes. Future studies should focus on various fuel grain diameters, NOS injector designs, pre- and post-combustion chambers, and different fuel grain geometries and compositions.

TABLE OF CONTENTS

Chapter Page

LIST OF TABLES

LIST OF FIGURES

CHAPTER I

INTRODUCTION

1.1 Introduction and Motivation

Hybrid rocket engine research and development is necessary to close the performance gap of solid and liquid rockets, because hybrid rocket engines traditionally have a lower thrust to weight ratio and specific impulse respectively. Chemical propulsion systems are the most well understood and used rocket propulsion systems among the major categories. Within this category there are three types: solid, hybrid, and liquid rocket engines. Since the 1930's the focus of chemical propulsion systems has been on solid and liquid rockets, but a newfound interest in hybrid rockets has taken hold. This interest is in part due to a hybrid rocket being chosen to power the second stage of Tier One, the winner of the 10-million-dollar Ansari XPRIZE. Hybrid rockets decrease the concerns around propellant handling, are easy to throttle up or down, and have a potential for a higher specific impulse when compared to solid engines. When compared to liquid engines, hybrid engines tend to reduce the mechanical intricacy, can contain solid metal additives, and have denser fuels. However, hybrid rocket engines traditionally have poorer performance when compared to solid and liquid in terms of thrust-to-weight ratio and specific impulse respectively. Therefore, this study aims at closing the gap and increasing the performance measures. Hybrid rocket engines are a type of rocket propulsion system that uses propellant in two different states of matter, one being solid and the other is either liquid or gaseous. The basic concept of a hybrid rocket propulsion system consists of a pressure vessel containing the fluid propellant, and the solid propellant placed in the combustion chamber separated by a valve. Figure 1

[1] serves as a reference for the basic design of a hybrid rocket engine.

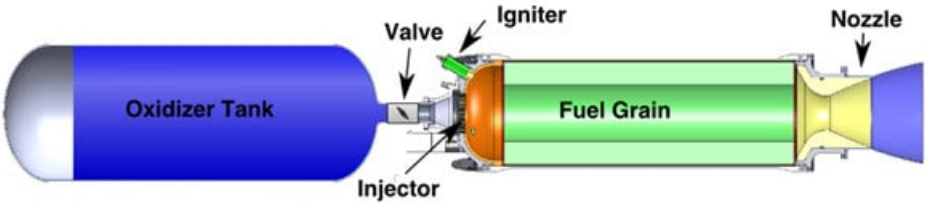

Figure 1: Basic Hybrid Rocket Configuration [1]

When thrust is desired the valve is opened and the fluid propellant flows into the combustion chamber where an ignition source is introduced. As it enters the combustion chamber, the fluid propellant is vaporized and reacts with the solid propellant. Typically, the fluid propellant is the oxidizer, and the solid propellant is the fuel. This is because solid oxidizers under-perform when compared to fluid oxidizers. The commonly used oxidizers in hybrid rocket engines are O_2, O_3, N_2O, N_2O_4, Inhibited Red Fuming Nitric Acid ($IRFNA$), and H_2O_2 [2]. The mission will be one of the main determining factors on the type of oxidizer used, another consideration in picking an oxidizer for hybrid rocket engines is the performance parameter, specific impulse (I_{sp}). Specific impulse and its determining factors will be explained in a later section; however, Figure 2 [2] shows the specific impulse of various oxidizers resulting from the mixture of the oxidizer and an hydroxyl-terminated polybutadiene solid fuel (HTPB).

Within a hybrid rocket engine, the solid fuel grain is most typically comprised of HTPB. HTPB is a polymer that is widely used in rocketry. In solid rockets it is the binding agent of the propellant but it has been found that HTPB would be a suitable fuel grain for hybrid rocket engines because of its ease of manufacturing and good mechanical properties for highly loaded grains [3]. However, there has been recent development in the composition of hybrid rocket fuel grains. One question is whether additively manufactured fuel grains, 3D printed fuel grains, could provide similar performance values while reducing the manufacturing time and involvement compared to that of an HTPB grain. These 3D printed fuel grains could be made of a large variety of materials, as well as having the potential for additives that will

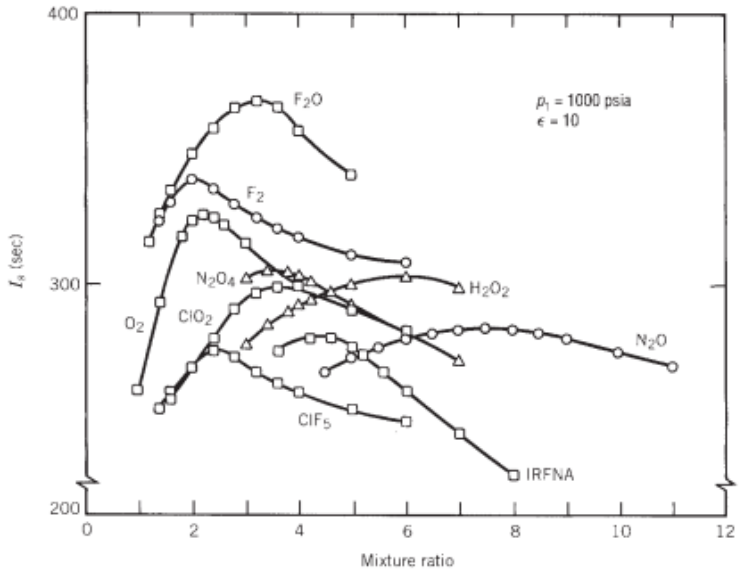

Figure 2: Vacuum Specific Impulse of Various Oxidizers Reacted with HTPB Fuel [2]

enhance the burning characteristics of the fuel grain [4]. Another opportunity for the 3D printed fuel grains to outpace its HTPB counterpart, is the numerous core geometries that can be made by a 3D printer; which could increase the performance of the overall system.

It is well understood that varying the throat area of a nozzle for a solid rocket will change the way in which the motor performs as a whole [5]. The variance in solid rocket motor performance is because of the effect nozzle throat area has on mass flow rate. However, there are few if any studies reviewing the effect of varying the mass flow rate for hybrid rockets. Although varying the mass flow rate of a hybrid rocket may seem like it would produce the same changes as a solid motor, this conclusion is yet to have been made. As mentioned before hybrid rocket engines have an influx of oxidizer, which is not the case in solid rocket engines, and this fact may change the way the exhaust gases interact with the nozzle producing unexpected performance characteristics. This, again, necessitates a study evaluating the performance of a hybrid rocket engine when the inlet mass flow rate of the oxidizer and the outlet mass flow rate of the nozzle is changed.

1.2 Research Objectives

The research objectives for this study are to design and construct a small-scale hybrid rocket test stand, as well as evaluating the effectiveness of the test stand in different configurations and conditions, using thrust as the primary figure of merit. This includes a NOS refill station; a LabVIEW VI to control ignition, opening of valves, as well as collecting thrust and specific impulse data. Thrust and specific impulse will be maximized by varying the outlet pressure of the regulator and areas of the orifice and nozzle respectively.

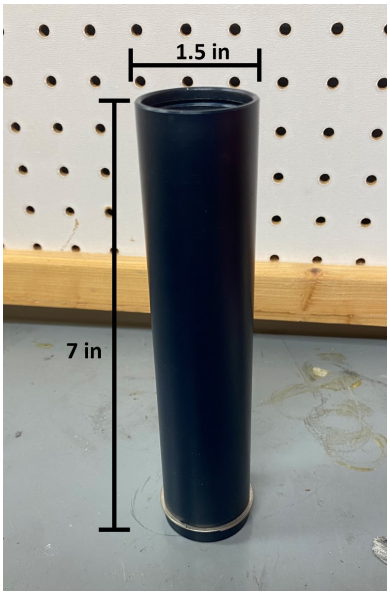

Figure 3: 1.5-in Hybrid Rocket Casing

To close the performance gap with other chemical rocket types a well-designed, accurate, portable, and novel test stand is needed. There are several reasons for a test stand, these reasons include: the advancement of the understanding of hybrid rocket technology, to evaluate and compare different engine designs, to develop new hybrid rocket fuels and oxidizers, and to support the design and development of hybrid rocket engines. A hybrid rocket test stand allows researchers and engineers to study the performance and behavior of hybrid rocket engines under controlled conditions. These studies can help to advance the understanding of hybrid rocket technology and its potential applications. A hybrid rocket

test stand can be used to evaluate the performance of different hybrid rocket engine designs, including those with different fuel formulations, nozzle designs, and other characteristics, which can help identify the most promising engine designs. A hybrid rocket test stand can be used to study the combustion characteristics of different hybrid rocket fuels and oxidizers. Propellant studies can help to develop new fuel and oxidizer combinations that have improved performance, safety, and reliability. A hybrid rocket test stand can be used to test and validate the design of hybrid rocket engines, including the engine's nozzle, combustion chamber, and other components. Increased testing can help to ensure that the engine will perform as expected and to identify and address potential design issues. The hybrid rocket engines developed for testing in this study involve high pressure NOS flowing from a 10-lb bottle, through a steel braided hose, solenoid valve, check valve and finally being injected into a 1.5-in (38-mm) diameter, 3.5-in long fuel grain with a 0.65-in core. The 7-in long 1.5-in diameter aluminum casing that holds the fuel grain can be seen in Figure 3 and is meant to serve as a reference for the size and scale of the motors used for this study.

CHAPTER II

BACKGROUND AND THEORY

2.1 Hybrid Rocket Engine Fundamentals

Rocket engines generally share a consistent set of key performance parameters. Typical performance measurables for hybrid rocket engines are thrust (F), specific impulse (I_{sp}), chamber pressure (P_c), burn time (t_b), characteristic velocity (C*), thrust coefficient (C_f), and burn rate (r_b) [6]. These parameters are most directly related to aspects specific to each rocket and configuration, especially with regards to nozzle geometry and propellant composition. Thrust is the propulsive force generated by the rocket engine and is measured in units of force, such as pounds or newtons. It is the key parameter that determines the acceleration of the rocket and is typically measured at the nozzle exit plane. Burn time is the duration of the rocket engine's operation, from ignition to shut down, and is typically measured in seconds. It is an important parameter for determining the total impulse produced by the engine and for comparing different engine designs. Burn rate is the rate at which the fuel is consumed by the rocket engine and is typically measured in units of mass per time, such as pounds per second or kilograms per second. It is an important parameter for calculating the total impulse produced by the engine and for determining the fuel requirements for a given mission. Specific impulse is a measure of the efficiency of the rocket engine and is typically expressed in units of seconds. It is the ratio of the thrust produced by the engine to the rate of fuel consumption, and it is an indicator of the amount of thrust that can be generated per unit of fuel. Total impulse is the total amount of thrust produced by the rocket engine over the duration of its operation and is typically measured in

units of force-time, such as pound-seconds or newton-seconds. It is an important parameter for determining the overall performance of the engine and for comparing different engine designs. Chamber pressure is the pressure inside the combustion chamber of the rocket engine, and is typically measured in units of pressure, such as pounds per square inch or pascals. It is an important parameter for determining the performance of the engine and for ensuring that the engine operates safely and reliably. Characteristic velocity is a measure of the exhaust velocity of the gases as they are expelled from the nozzle of the rocket engine, and is typically expressed in units of velocity, such as feet per second or meters per second. It is an important parameter for calculating the specific impulse of the engine and for determining the performance of the engine. Thrust coefficient is a dimensionless parameter that describes the efficiency of the engine's nozzle and is calculated as the ratio of the thrust produced by the engine to the square of the chamber pressure. It is an important parameter for determining the performance of the engine and for comparing different engine designs. In summary, the key performance parameters of a hybrid rocket engine are thrust, burn time, burn rate, specific impulse, total impulse, chamber pressure, characteristic velocity, and thrust coefficient. These parameters are important for evaluating the performance and efficiency of the rocket engine and for comparing different engine designs.

When considering the thrust produced by a rocket motor, it is important to consider the control volume in question. For the purposes of this analysis, a NOS bottle is secured to the test stand and connected to the forward end of the fuel grain casing, and the casing is secured to flat plates attached to linear bearings with the thrust ring of the casing pressing up against the flat plates. Drawing the control volume so that only the influx of oxidizer, the solid fuel grain, and load cell are included will result in the inclusion of propellant temperature, pressure, and mass flow properties within the casing. It is important to also note the inclusion of pressure forces at the nozzle exit as depicted in Figure 4.

Referring to Newton's second law of motion in Equation 2.1.1, and assuming a one dimensional and steady flow field along with observing there are no influx properties coming

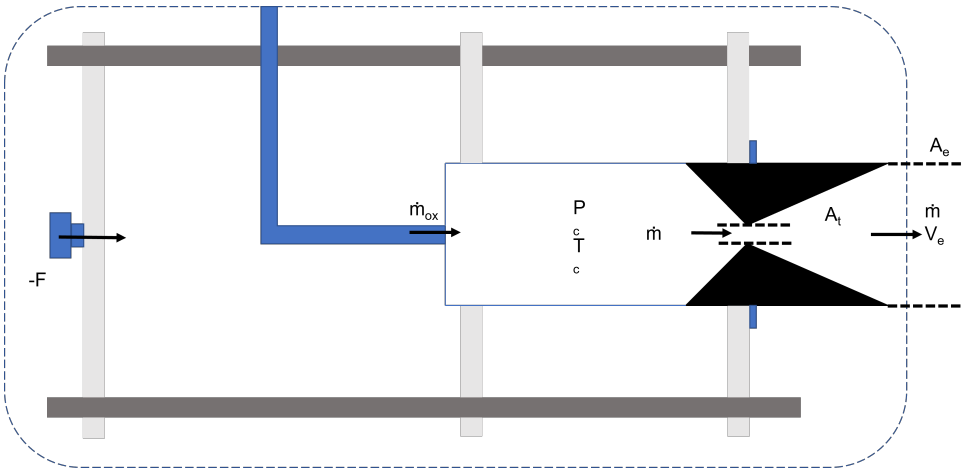

Figure 4: Hybrid Rocket Control Volume

into the control volume, the momentum equation can be simplified and ideally described as the sum of momentum and pressure forces exiting the control volume through Equation 2.1.2, using the expression for mass flow rate defined in Equation 2.1.3.

$$\frac{1}{g_c}\frac{\partial}{\partial t}\int\int\int_{cv}\vec{V}\rho d\forall + \frac{1}{g_c}\int\int_{cs}\vec{V}\rho(\vec{V}\cdot\hat{n})dA = \Sigma\vec{F} \tag{2.1.1}$$

$$F = \frac{\dot{m}\cdot V_e}{g_c} + (P_e - P_a) * A_e \tag{2.1.2}$$

$$\dot{m} = \frac{g\cdot P_c\cdot A_t}{C^*} \tag{2.1.3}$$

The first term on the right side of Equation 3 is a measure of how much momentum the rocket motor is imparting, while the second term accounts for pressure thrust that is a result of nozzle performance. The momentum term will account for most of the thrust produced while the pressure term can be positive, negative, or zero depending on if the nozzle is under, over, or perfectly expanded. Perfect expansion results in ideal nozzle performance and indicates that the nozzle exit pressure is equal to ambient pressure. This results in the pressure terms within the steady and one-dimensional thrust equation to be equal to zero. Figure 5 [7] serves as a visual representation for the different modes of nozzle performance.

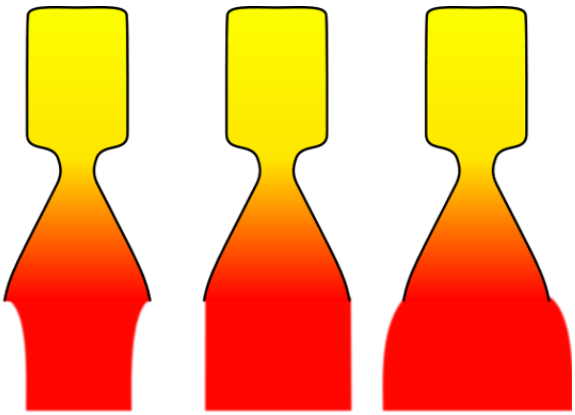

Figure 5: Over Expanded (Left), Perfectly Expanded (Center), and Under Expanded (Right) Nozzles [7]

Specific Impulse (I_{sp}) is a measure of a rocket's thrust per unit of propellant gas weight-flow exiting the nozzle. In the case of hybrid rocket engines, this can also be described as the ratio of total impulse to propellant mass consumed throughout the duration of its burn. It is in this area that traditionally hybrid rockets perform better than other forms of chemical rocket propulsion systems as it doesn't require as much propellant weight to produce comparable amounts of thrust. The equation for specific impulse can be observed in Equation 2.1.4 below.

$$I_{sp} = \frac{F}{\dot{w}} \tag{2.1.4}$$

Characteristic velocity (C^*) varies based on the propellant composition, as expressed in Equation 2.1.5, and is used to get a sense for the amount of energy available. Characteristic velocity can be expressed as a function of propellant chamber pressure, nozzle throat area, and mass flow rate or as a function of propellant chemical compositional characteristics that are specific to that particular propellant formulation.

$$C^* = \frac{P_c * A_t}{\dot{m}} = \sqrt{\frac{R_u * T_c}{Y * MW}} * [\frac{2}{Y} + 1]^{\frac{-(Y+1)}{2*(Y-1)}} \tag{2.1.5}$$

A rocket engine's burn rate (r_b) is a function of chamber pressure and a set of empirical

constants known as the burn rate coefficient (a) and burn rate exponent (n) as shown in Equation 2.1.6. An engine's burn rate coefficient and exponent can be determined experimentally and is unique for each propellant composition. It is important to note that burn rate is not unitless and actually has Imperial units of $\frac{in*psi^n}{s}$, or $\frac{cm*MPa^n}{s}$ for SI units.

$$r_b = a * P_c^n \tag{2.1.6}$$

The burn time (t_b) of a motor is determined through use of the general thrust profile exhibited throughout the entirety of its burn. A motor's thrust profile will typically portray an initial rise, followed by some sort of sustained thrust output, and end with either a slow or quick deterioration in thrust produced. Within this study, burn time is characterized to start at the 10% maximum thrust value exhibited on the initial rise, and end at the 10% total maximum thrust value during thrust deterioration, as shown in Figure 6 [8] below.

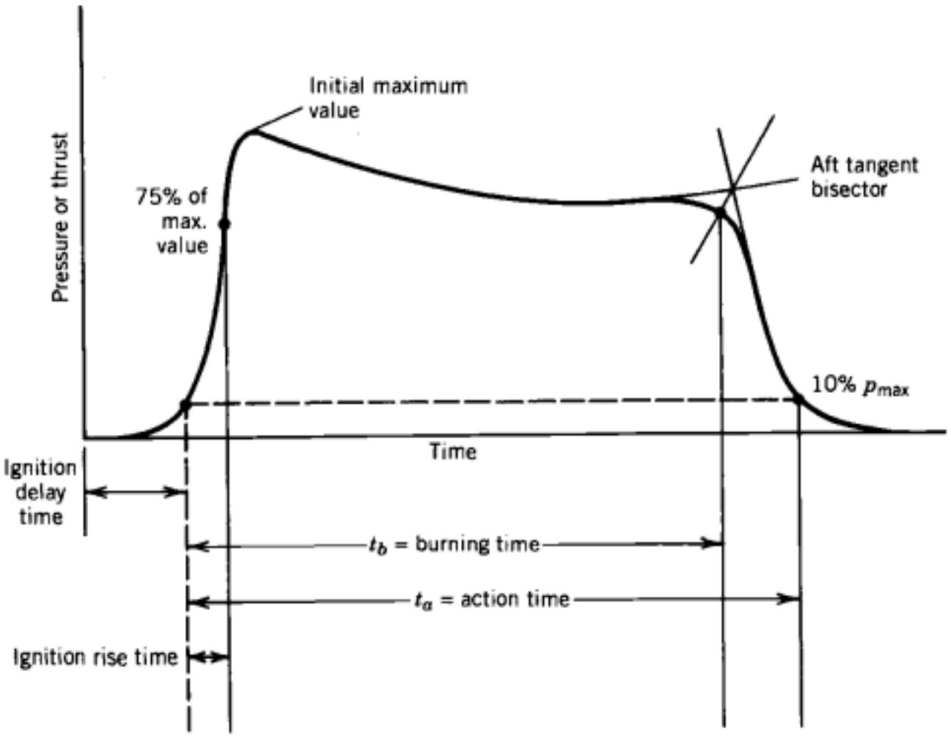

Figure 6: Definition of Engine Burn Time [8]

The chamber pressure (P_c) within the aluminum casing is a key parameter of interest

because it determines how fast the solid fuel grain will burn. The higher the chamber pressure the faster an engine's burn rate will be. Chamber pressure is also important for safety purposes. Engine casings must be built with the intent of being able to contain the forces being exerted onto the casing from gases being burned and accelerated through the nozzle. Assuming a fixed nozzle geometry, nearly constant pressure across the length of the solid fuel grain, and that mass flow through the nozzle varies minimally across the engine's burn time ($\dot{m}_{in} = \dot{m}_{out}$), instantaneous chamber pressure can be solved as shown in Equation 2.1.7.

$$P_c = [\frac{a * \rho_p * A_b * C^*}{g * A_t}]^{\frac{1}{(1-n)}} \tag{2.1.7}$$

From this, the combination of fluid and solid propellant formulation will hold burn rate coefficient, burn rate exponent, propellant density, and characteristic velocity constant, leaving the profile of the engine's chamber pressure across its burn time to mirror the instantaneous total burning surface area.

Total impulse is measured through taking the integral of thrust produced over the burn time of the rocket motor and is used to quantify the total amount of energy exerted by propellant. Simplification of this integral can be done if either thrust or specific impulse is assumed to be constant as shown in Equation 2.1.8.

$$I = \int_0^{t_b} F * dt = F * t_b = I_{sp} * m_p \tag{2.1.8}$$

Finally, thrust coefficient is a dimensionless parameter used to indicate the amount of thrust produced relative to its chamber pressure and throat area as expressed in Equation 2.1.9. Thrust coefficient is maximized under the condition of perfect expansion, making it a good metric for measuring aspects related to nozzle performance.

$$C_f = \frac{F}{P_c * A_t} \tag{2.1.9}$$

2.2 Hybrid Engine Pros and Cons

Hybrid rocket engines have several advantages and disadvantages compared to other types of rocket engines, such as liquid rocket engines and solid rocket motors. One of the main advantages of hybrid rocket engines is their simplicity and low cost. Because the fuel is solid and the oxidizer is liquid or gaseous, the engine does not require the complex plumbing and turbopumps that are used in liquid rocket engines. This makes the engine simpler and cheaper to manufacture, maintain, and operate. Another advantage of hybrid rocket engines is their safety and reliability. Because the fuel is solid, it is not as susceptible to leaks or spills as liquid fuel. This makes the engine safer to handle and store, and it reduces the risk of accidents or fires. Additionally, the solid fuel can be easily ignited and extinguished, which allows the engine to be throttled and shut down as needed. A third advantage of hybrid rocket engines is their performance and efficiency. Because the fuel and oxidizer are mixed in the combustion chamber, the engine can achieve high combustion efficiency and generate high specific impulse. This makes the engine capable of generating high thrust and high specific impulse, which are important for rocket propulsion [9].

There are several disadvantages to using hybrid rocket engines. These disadvantages include limited by the properties of the solid fuel, difficult to control and modify, relatively low thrust-to-weight-ratio, and limited data and experience. The performance of the hybrid rocket engine is limited by the properties of the solid fuel, which must be able to burn evenly and consistently to produce stable combustion. This can be challenging to achieve, and it can limit the engine's performance and efficiency. Because the solid fuel is difficult to control and modify once it has been cast or molded, it can be challenging to make changes to the engine's performance or characteristics. This can make it difficult to optimize the engine for specific missions or requirements. The thrust-to-weight ratio of hybrid rocket engines is typically lower than that of other types of rocket engines, such as liquid rocket engines or solid rocket motors. This can limit their potential applications and make them less suitable

for certain missions or requirements. There is relatively limited data and experience with hybrid rocket engines compared to other types of rocket engines. This can make it difficult to predict their performance and reliability, and it can pose challenges for mission planners and designers. These disadvantages can limit their potential applications and make them less suitable for certain missions or requirements [10]. Figure 7 [1] shows the physical differences between the three types of chemical rockets.

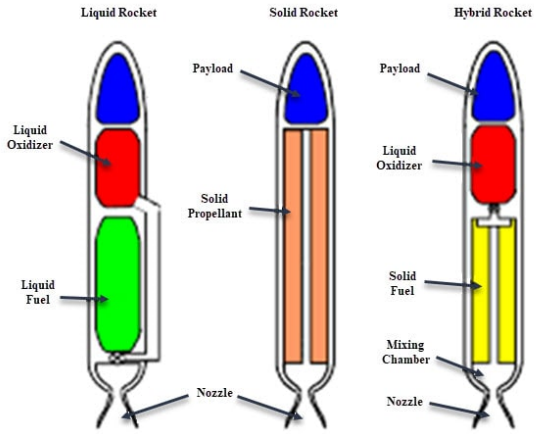

Figure 7: Liquid Rocket (Left), Hybrid Rocket (Middle), Solid Rocket (Right) [1]

Despite the disadvantages of hybrid rocket engines, their advantages make them an attractive option for many applications. The simplicity and low cost of hybrid rocket engines make them appealing for small satellite missions, research and development projects, and other applications where cost and complexity are important considerations. Additionally, the safety and reliability of hybrid rocket engines make them well-suited for missions that require high levels of safety, such as human spaceflight or missions with strict safety regulations.

2.3 Hybrid Engine Types

Chemical propulsion can encompass a wide range of rocket types and compositions, but at its core all chemical type propellants require an oxidizing agent and a fuel to facilitate the proper chemical reaction. Hybrid rocket engines can exist in a multitude of ways and are defined by the type of fuel and oxidizer they use. Some of the most common types of

hybrid rockets are solid fuel hybrid engines, mono-propellant hybrid engines, bi-propellant hybrid engines, cryogenic hybrid engines, and hybrid-thermal engines. Solid fuel hybrid engines are characterized by using a solid fuel, such as rubber or plastic, and a liquid or gaseous oxidizer, such as NOS or hydrogen peroxide. These types of hybrid rocket engines are the most used. Mono-propellant hybrid engines use a single chemical, such as hydrazine or hydrogen peroxide, as both the fuel and oxidizer. The fuel is typically a liquid that is pressurized and stored in a tank, and the oxidizer is typically a gas that is stored in a separate tank. Bi-propellant hybrid engines can be like solid fuel hybrid engines in that the fuel is solid and the oxidizer is a fluid, but some other types of bi-propellant hybrid engines can have fluid fuel and solid oxidizer. These types of hybrid engines can be difficult to make and store depending on the nature of the solid oxidizer. Cryogenic hybrid engines are also relatively like the solid fuel hybrid engines in that the fuel is a solid and the oxidizer is fluid; however, in a cryogenic hybrid engine the oxidizer is extremely cold and produces exhaust gases well below 0 degrees Fahrenheit. These engines have great advantages, but with their nature being cryogenic, it can be incredibly difficult to store. Hybrid-thermal engines are once again similar to solid fuel hybrid engines in the propellant types, but they are designed to burn at a much higher temperature, in the 4,500-5,500-degree Fahrenheit range. This high performing temperature allows the engine to produce a high specific impulse which could be necessary in applications that need high thrust over a long period of time.

Each type of hybrid rocket engine has its own pros and cons; however, for this study the solid fuel hybrid engine was chosen. This is due to the solid fuel hybrid engine's simplicity, reliability, performance, and cost. Solid fuel hybrid rocket engines are generally simpler to design and build than other types of hybrid engines, which makes them more attractive for this study. Solid fuel hybrid engines are also generally more reliable than other types of hybrid engines because they don't require the use of complex systems to function. This makes them more suitable for this study where reliability is a major concern as students at Oklahoma State University are beginning the endeavor towards high powered hybrid

rocketry. Solid fuel hybrid engines can deliver high levels of thrust and have a high specific impulse, which makes them suitable for use in a variety of applications. Solid fuel hybrid engines are generally less expensive to manufacture than other types of hybrid engines, which makes them the most attractive option for this study.

2.4 Hybrid Engine Composition

As mentioned before, the key components to any chemical rocket engine include oxidizer and fuel. Depending on the type of hybrid rocket engine chosen the oxidizer and fuel may come in a variety of forms; however, for the solid fuel hybrid engine, as described in its name, the fuel is solid, and the oxidizer is in fluid (liquid or gaseous) form. There are also other ingredients that should be noted that could act as plasticizers, curing agents, and opacifiers that also serve as several other additive roles. The addition, subtraction or substitution of these ingredients can have large impacts on overall motor performance. Another key point in deciding the type of fuel or oxidizer to use in the hybrid rocket system is the type of mission or testing the rocket will be used for. The mission requirements will help determine and guide the choice of the propellants. Different oxidizers and fuels can add features like higher performance and long storability with the typical concessions of higher cost or non-environmentally friendly exhaust products.

When looking at hybrid rocket solid fuels there are many choices that can be made. Fuels can be made of ingredients that have to be cured, machined into shape, or created on a 3D printer. The different ways to make fuel for hybrid rocket is dependent upon the speed required of production, ordering of materials, extraneous machines required, and ease of production. Although these factors carry much weight, the most important part of hybrid rocket solid fuel grains are the composition. If the grain must be cast; order of material introduction and timing of steps can cause variations in propellant properties that will have a large impact on overall engine performance and consistency. When looking at machining a solid fuel grain the purchasing of materials and the machine to cut the grain into shape

are the most critical aspects. Typically, the machine will be of a high cost and require a specialist to operate. When it comes to 3D printing fuel grain, caution must be taken when designing the fuel grain due to tolerance limitations of the 3D printer; however, the ease of use and designing a fuel grain makes 3D printing the best option when it comes to making hybrid rocket solid fuel grains.

2.4.1 Oxidizer

In hybrid rocketry, one of the most difficult tasks is to choose the type of oxidizer that will help to power the engine. There are many considerations when it comes to oxidizers for hybrid rockets: performance characteristics, storability, cost, stability, and ease of use. Some different types of oxidizers are O_2, O_3, N_2O, N_2O_4, $IRFNA$, and H_2O_2. Each oxidizer has its pros and cons as can be seen in Figure 2 as well as in Table 1 [2].

Oxidizer	Type	Boiling Point ($^\circ C$)	Density (g/cm^3)	$\Delta_f H^a$
O_2	Cryogenic	-183	1.149	-3.1
O_3	Cryogenic	-112	1.614	+30.9
N_2O	Cryogenic	-88	1.226	+15.5
N_2O_4	Storable	+21	1.449	+2.3
IRFNA	Storable	+80 to +120	1.583	-41.0
H_2O_2	Storable	+150	1.463	-44.8

Table 1: Thermochemical Properties of Selected Oxidizers Reacted with HTPB Fuel [2]

While all these oxidizers could have been studied, the choice came down to three different types of oxidizers: O_2 (LOX), N_2O (NOS), and H_2O_2 (Hydrogen Peroxide). Liquid oxygen is a widely used cryogenic oxidizer in the space launch industry; it is relatively safe and delivers high performance at a relatively low cost. Hydrogen Peroxide received a lot of interest from scientists in the early days of rocketry, but that has decreased until today. Hydrogen Peroxide is similar to LOX in its requirements for handling and fire safety; however, it requires less

mechanical intricacy than LOX within the rocket [11].

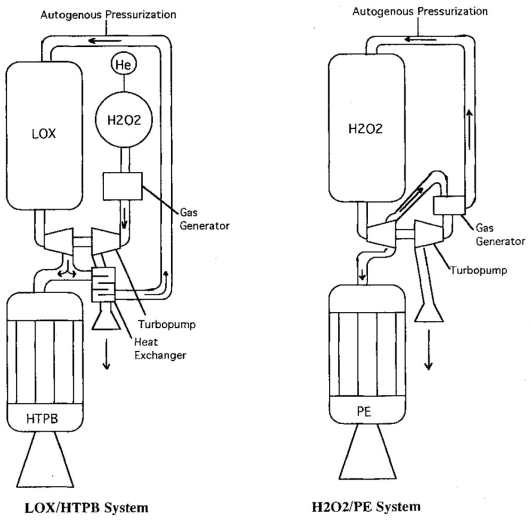

Figure 8: LOX vs. Hydrogen Peroxide Cycle Comparison [11]

The final oxidizer consideration for this study was NOS. NOS is most popular for its use in street racing vehicles as it increases the power output of an engine. NOS aides vehicle engines by increasing the amount of fuel that can be burnt because it increases the supply of oxygen to the engine. However, it has gained interest recently as a potential oxidizer for hybrid rocket engines. NOS has many properties that make it a quality candidate for a variety of missions. It is inert, has a long shelf life, a good density, high vapor pressure, and good overall combustion characteristics [12]. One of the key reasons for NOS being investigated as a hybrid rocket oxidizer is its advantage of being able to self-pressurize. Many hybrid rocket demonstrations in recent years have taken advantage of the self-pressurizing ability of NOS including: SpaceShipOne and SpaceShipTwo [13], HEROS 3 [14], the rocket test sled trials of Muroran Institute of Technology [15], TiSpace [16], and finally the sounding rockets of Space Forest Ltd. [17]. NOS is also easy to obtain and store, making it a preferable oxidizer for this study.

Although NOS has great qualities with a good track record in rocketry, the handling of NOS can be tricky. With guidance from SpaceDev Inc. and Nitrous Outlet testing, and use of NOS has been and will continue to be done with extreme care [12]. With all of the NOS

Figure 9: SpaceShipOne Test Flight [13]

thermochemical and decompositional properties taken into account, as well as the inherent safety and self-pressurizing benefits. NOS is the perfect oxidizer for the introduction of Oklahoma State University into the hybrid rocket sphere.

2.4.2 Fuel

Along with the oxidizer of a hybrid rocket engine, the fuel is the other half of the combustion process. Traditionally, the fuel choice for hybrid rocket engines has been any solid hydrocarbon material because they can provide the necessary hydrogen and carbon molecules to create high flame temperatures. This leads to the common use of HTPB, carboxyl-terminated polybutadiene (CTPB), and polybutadiene acrylonitrile (PBAN) [2]. HTPB has been the preferred fuel of choice for many hybrid rocket designs because of the industry's familiarity with its chemical and structural properties. HTPB must be mixed from its liquid components, degassed in a vacuum, then cast and cured in a fuel grain mold.

However, some of the biggest issues with these types of solid fuel grains are the labor-

intensive manufacturing process and the limited geometry for internal combustion ports. These two problems with the traditional "cast and cure" method truly capped the ability of hybrid rocket engine designs. Another issue with the traditional method of creating hybrid rocket fuel grains can be the inconsistency of the mixture, the environment in which the grain is casted, the length of time for the curing process, and the amount of residual gas left in the mixture. With the recent advancements of technology, more plastic-like materials have been used in research studies. Finally, with the advent of additive manufacturing, more specifically, fused deposition modeling (FDM) 3D printers opened the door to more complex port geometries, less labor-intensive manufacturing processes, and various other parameters like infill percentage, internal print structure, layering techniques, and a wide range of materials. FDM 3D printers are considered additive because they lay down material layer by layer on top of previously printed material. FDM 3D printers have multiple advantages over the "cast and cure" method when it comes to manufacturing, FDM 3D printers produce negligible waste because it is additive. Also, depending on the material being printed there is little to no post-processing or retooling on the print when compared to typical subtractive methods, that start with a whole piece and trim it down to the desired shape [18]. This additive manufacturing process is adaptable, scalable, automated, free-form, and repeatable making it attractive for processes like hybrid rocket fuel grain development.

There are many types of filaments on the market today that can be used for 3D printing like PLA, Acrylonitrile Butadiene Styrene (ABS), Acrylonitrile Styrene Acrylate (ASA), Polyethylene Terephthalate Glycol (PETG), Nylon, as well as some non-plastic materials. The structural, thermal, and mechanical properties of some of these materials are include in the following table [19].

ABS is a recyclable and inexpensive thermoplastic that has several mechanical properties that make it attractive as a hybrid rocket fuel. ABS can be formed into any desired shape allowing for complex interior passages for the fluid oxidizer to flow, this is true for almost all FDM filaments. One of the big advantages of ABS is the structural modulus and tensile

Material	Structure	$\rho\ (g * m^{-3})$	σ (MPa)	Print Temperature $(^{\circ}C)$
ABS	Non-crystalline, amorphous	1010	55	$220 - 260$
ASA	Non-crystalline, amorphous	1000	40	$220 - 250$
PLA	Moderate degree of crystallinity	1225	63	$190 - 220$
PETG	Moderate degree of crystallinity	1230	50	$230 - 250$

Table 2: Structural, Thermal, and Mechanical Properties of Select FDM Filaments [19]

yield strength [20]. ASA is very similar to ABS, but it offers increased weather resistance and can be more expensive than its counterpart. PETG has excellent mechanical properties but would not be a great hybrid rocket fuel grain. The most intriguing of these FDM filaments is PLA. PLA is relatively like ABS in its mechanical properties; however, the biggest advantage it has over ABS is the limited toxicity it produces when combusted. ABS is known for high levels of toxicity during the thermal degradation process, while on the other hand, PLA is eco-friendly and biodegradable. PLA, like ABS, is an incredibly cheap filament to purchase and is considered the most widely available filament. PLA is a thermoplastic polyester with the backbone formula ($C_3H_4O_2$) and is formally obtained by the condensation of lactic acid from fermented corn starch. Thermal decomposition of PLA relies on a complex phenomenon that leads to lighter molecules and linear or cyclic oligomers with different molecular weights and lactide. Table 3 [21] presents the material properties of PLA compared with ABS and a traditional hybrid rocket fuel, HDPE.

As seen in Table 2 and Table 3, there is a slight variation in the densities of PLA and ABS. This variation could be due to slight differences in the environments and ways in

Material	Repeating Unit	Ignition Temperature, $(^{\circ}C)$	$\rho\ (g * m^{-3})$
HDPE	(C_2H_4)	340	970
ABS	$(C_3H_3N, C_4H_6, C_8H_8)$	466	1030
PLA	$(C_3H_4O_2)$	388	1240

Table 3: Material Properties of HDPE, ABS, and PLA [21]

which the materials were tested. All the properties presented in Table 3 help to justify the case for PLA as a possible fuel for hybrid rocket engines. The density of PLA is much higher than that of the other two materials compared in the table. With a higher density material there would be more mass in the same size and shape of fuel grain, this leads to more propellant being able to be burnt and a higher energy density of the material. PLA also has a medium ignition temperature when compared to that of HDPE and ABS. A high ignition temperature is the least desirable because it requires a high amount of energy to begin the combustion process. For this property HDPE beats out FDM filaments, but PLA still has the lowest ignition temperature of the two FDM filaments. The lower ignition temperature of PLA would allow for a shorter ignition time and less energy to combust the PLA fuel grain. Additionally, primary toxic gases like CO and HCN can be generated from the thermo-oxidative degradation of ABS. While PLA has been known to emit harmful combustion products, such as polycyclic armoatic hydrocarbons (PAH), it releases them at considerably lower levels than other plastic materials [22] and produces little to no remaining residue. PLA can be combusted without producing harmful chloring-containing chemicals or heavy metals because it only contains carbon, oxygen, and hydrogen atoms. This point, about the residue, is desirable for PLA's use as a hybrid rocket fuel because the entirety of the fuel grain can be burnt without leaving a residue or creating a harmful impact on reusable rocket casings [23].

A study on the thermal degradation and combustion properties of popular biodegradable

polymers found that PLA has an endothermic peak temperature of $382.6°C$ in a nitrogen environment and a peak temperature of $385.2°C$ in an oxygen environment. The similarity of the peak temperatures in the two environments show that PLA could be a one-step decomposition mechanism. The study also shows a Fourier transform infrared (FTIR) spectra that displays CO_2 as the dominant product during the thermal decomposition of PLA in an oxygen environment whereas in a nitrogen environment $C = O$ is the main product produced. The FTIR images also show there are a few, small, decomposed molecules below $320°C$ [24]. This study is especially interesting because it compares the degradation of PLA in an oxygen environment to that of a nitrogen environment: the two elements that make up NOS. There are no other studies related to the combustion or thermal decomposition of PLA.

Taking all the information about more classical hybrid rocket fuels and the potentially new hybrid rocket fuels. The desired hybrid rocket fuel grain material for this study is PLA. It is easy to work with; easy to obtain; its thermal, chemical, and mechanical properties are well understood; PLA has a long shelf life; and finally it is the cheapest hybrid rocket fuel on the market.

2.4.3 Other Additives

Even though there are no other additives used for this study, it is important to note the potential for additives in hybrid rocket engines. The most notable of these, and discussed previously, is the ability to impregnate the solid fuel grains with metal particulates. Adding metal into solid rocket motors is known to increase the engine's overall performance and consistency [25]. Some studies have focused on adding aluminum particles to hybrid rocket engine fuel grains. In these studies it has been shown that aluminum particles can increase the specific impulse, volumetric heat of oxidation and radiative heat transfer, as well as increasing the regression rate in HTPB engines by up to 40% [26, 27]. Figure 10 shows nano-aluminum particulates in an HTPB fuel grain.

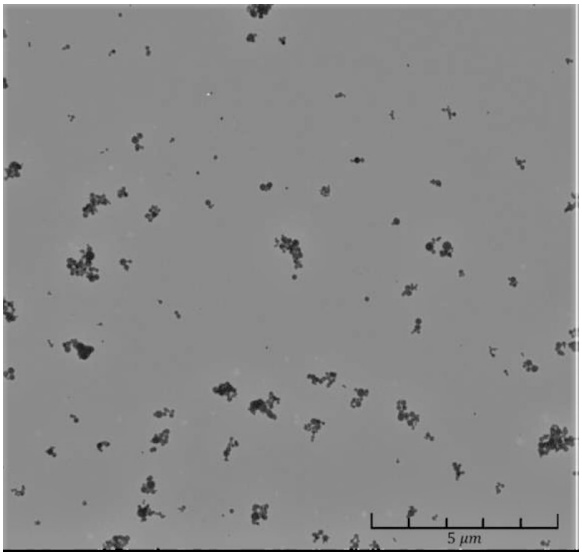

Figure 10: TEM Image of a Nano-Aluminum Particle Dispersion in HTPB Grain [27]

While these studies focus on the traditional HTPB fuel grain, it is possible to purchase certain FDM filaments infused with aluminum powder or other metals. Adding metals also increases the regression rate of hybrid fuel grains. Regression rate is the rate at which the solid fuel is converted to gaseous vapor [28]. This means that a higher regression rate is more desirable for higher impulse requirements. The increase in regression rate, when aluminum is added, is due to the energy release from metal oxidation and enhanced radiation heat fluxes from the flame area back to the solid fuel's surface.

The only "additive" selected for this study is the igniter. The igniter is technically not an additive to either the oxidizer or the fuel grain; however, it is the key to start the combustion process. Without the igniter the solenoid valve of the NOS could be opened, and the NOS could flow freely over the port surface of the PLA without creating a chemical reaction. The igniter provides the necessary heat source/activation energy to ignite the engine and begin combustion between the fuel and the oxidizer. The igniter used for the study is composed of two lead wires wrapped together on one end and dipped in pyrogen, as seen in Figure 11 [29]; while the other end of the leads is stripped and connected to an electrical source. This electrical source will send a signal to the end of the wire dipped in pyrogen when ignition is

desired. Pyrogen is essentially a solid rocket motor mixture that will not only increase the temperature inside the combustion chamber, but also burn a small amount of solid propellant to help mix the oxidizer and fuel together.

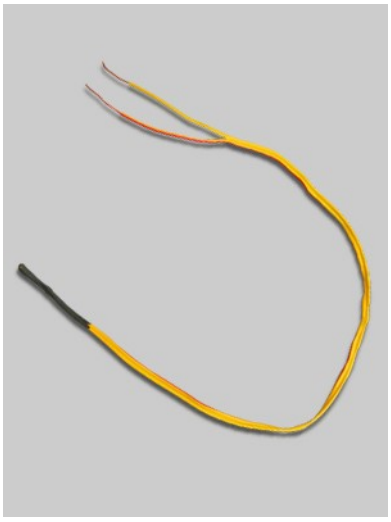

Figure 11: Sample Hybrid Rocket Engine Igniter [29]

While this study implements a single use igniter, it is important to note that depending on the design of the combustion chamber, there is a possibility to have an igniter which can have multiple ignitions. This is useful in situations where hybrid rockets are used as attitude stabilizers on space vehicles [30]. Although, having the ability for multiple ignitions is good, it can create increased mechanical intricacies in the combustion chamber design.

2.5 Propellant Manufacturing

With the aforementioned oxidizer and fuel, NOS and PLA respectively, a more in-depth approach will be taken to discuss manufacturing of solid and liquid propellant. Hybrid rocket engine's fuel and oxidizer systems must be manufactured with that idea that its propellant must be able to maintain structural integrity throughout any handling or storage that may take place prior to ignition, as well as being able to endure the loads and vibrations during testing. For the oxidizer system this entails the main "mother" bottle, small testing bottle, fittings, and hoses. For solid fuel grains this encompasses potentially long shelf time and any

dropping or physical damage to the propellant by personnel as well as the way in which the PLA filament is printed on the 3D printer.

2.5.1 Liquid Oxidizer System

NOS is a compressed gas that requires careful handling and use. In this study, NOS will be transferred from a large 50-lb "mother" bottle to a smaller 10-lb testing bottle, and finally it will be released from the testing bottle into the combustion chamber of the hybrid rocket engine. To complete this task in an efficient but safe manner; proper fittings, hoses, and scales were used. The research and reasoning for these materials will be explained here.

NOS should be stored in a steel tank ranging from a 5-lb or 10-lb bottle all the way up to a 50-lb bottle. For this study a 50-lb NOS bottle was selected. A 50-lb bottle would be enough to complete all the testing for this study. However, for the test stand to be portable it was decided a smaller refillable bottle would be needed. Some of these smaller bottles include 5-lbs, 10-lbs, or 15-lb bottles. The 5-lb bottles are great for single use in cars and are lighter than the other size bottles, but they would limit the number of hybrid rocket engine tests that could be completed on a single fill. This would require a heightened oxidizer manufacturing time and a potential to waste more NOS due to the refilling procedures which call for a small amount of NOS to be released each time the small bottle is refilled. The 15-lb bottles were also an option for the test stand. This size would allow for more tests per refill, but this could also mean the NOS pressure in the bottle could drop significantly during the test. If the pressure in the bottle drops below the chamber pressure inside the rocket casing, back pressure could completely stop the flow out of the bottle and therefore end the combustion process in the chamber. The other problem with the 15-lb bottle is the cost, whereas the 10-lb and 5-lb bottles are less expensive. This leaves the 10-lb bottle as the best choice. It provides enough NOS for multiple tests while being able to keep a safe bottle pressure, and comes at a reasonable price. Figure 12 [31] provides a reference for the size and scale of some various sizes of small NOS bottles.

Figure 12: Various Sizes of NOS Bottles [31]

To transfer the oxidizer from the large "mother" bottle to the small test bottle a refill station was deemed necessary. There are a few different brands of NOS refill stations, but for the most part they all contain the same basic components: a pump, air-water separator, NOS filter, steel braided hoses to connect the bottles to the pump, and a scale. The selected refill station includes multiple hoses, cut off valves, and National Pipe Taper (NPT) to Army-Navy (AN) fittings, making this the preferred brand for the refill station. During the refill process, all valves are opened and the NOS flows smoothly from the large bottle to the smaller bottle. If the flow of oxidizer slows, a compressed air hose is attached to the pump and begins to force the oxidizer from the large bottle to the small bottle. Two other components of the refill station that were added to aid in the refill process: a bottle stand and a "mother" bottle heater. The bottle stand would help the refill process because it inverts the "mother" bottle from the upright position to an upside-down position; in essence, creating a gravity fed system. The other component, the "mother" bottle heater, is like a heating blanket that wraps around the 50-lb bottle and warms it. This warming of the bottle will increase the pressure inside the large bottle and help to force the NOS out of the large bottle into the

small test bottle. A sample image of this setup can be seen in Figure 13 [32].

Figure 13: Sample of NOS Bottle Stand and Heater [32]

Although all the hoses and fittings for the refill station were provided with the purchase of the refill station, extra supplies were required for the actual hybrid rocket test stand. The actual components purchased, and the setup of the stand will be described in more detail in Chapter 4; however, it is important to note here the research behind these purchases. All hoses and fittings used on the test stand should be rated for at least 1000 psi. This pressure rating was decided upon because the NOS testing bottle will not be filled to a higher pressure than this, and the pressure inside the combustion chamber will not exceed this pressure either. Also, fittings and hoses that are rated for higher than 1000 psi are extremely expensive and difficult to obtain through regular material providers like McMaster Carr. All fittings will be made of copper due to their extreme pressure and temperature resistance and long-lasting life. The oxidizer delivery design will be described in more detail in the following chapter.

2.5.2 Solid Fuel

As previously discussed, hybrid rocket solid fuel grains are traditionally manufactured through the cast and cure method. This conventional method begins by determining the amount of each ingredient needed on a per mass basis. The next step would be to weigh out those ingredients as determined in the previous step, and then mix the ingredients together until they look well mixed. Then the mixture will be placed in a vacuum chamber to remove all air pockets. Once the mixture has been degassed in the vacuum chamber, the casting tube is prepared by spraying mold release on the interior surfaces to be able to separate the cured grain from the casting tube. The mixture is then poured into the casting tube and left to cure. The curing time for a typical HTPB hybrid rocket fuel grain is 5 days when left at room temperature [33]. This labor and time intensive process is not ideal.

While on the other hand, 3D printed fuel grains are quite easy, involve little to no intervention, can be done in the background, and depending on the fuel grain geometry or infill percentage take far less time to complete. Both methods can be used to make large batches of solid fuel grains, but even with this being equal batch 3D printing still has the advantage in time of creation. A more in-depth discussion of 3D printing will be had in the following subsections.

Solid Fuel Manufacturing

Now that additive manufacturing has become a big part of almost every technical industry, people are researching ways to use additive manufacturing that might not have been expected, like in this study. FDM 3D printers are incredibly useful and efficient in printing intricate structures that would otherwise be difficult to manufacture. FDM printers take a polymer-based filament and force it through a heated nozzle, which is hot enough to melt the material and deposits the filament in 2D layers on the build platform. While the deposited filament layer is still warm, another layer is placed on top, and continued until the print is complete. Because the layers are still warm when deposited onto each other, the layers fuse

together to create a three-dimensional part. Figure 14 [34] shows how the hot end of the 3D printer works.

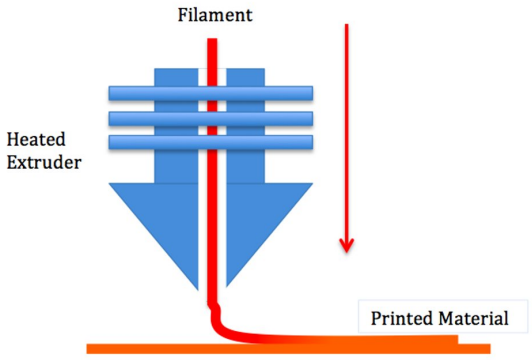

Figure 14: Sample FDM Print [34]

Before the printing process can begin it is important to understand what is being printed, and how the 3D printer knows what to do. 3D printing begins with computer-aided design (CAD) software, for this study SOLIDWORKS is the software of choice, but there are many others that can be used as well. In the CAD software, the designer will set the physical dimensions and the shape of the fuel grain to be printed. Once completed, the file should be saved as a standard tessellation language (STL) file. The STL file is then opened in a slicing software. Slicing softwares act as the link between the digital model and the physical model. It takes the digital model and converts it into physical steps for the 3D printer to take. The slicing software used for this study is Cura. Within Cura the designer can select the type of printer being used, the infill percentage, the temperature of the nozzle and heated bed (if the printer has a heated bed element), and many more options. Changing the infill percentage only changes how much of the interior volume of the print is filled with PLA, it does not affect the exterior structure of the fuel grain. The best range for PLA printing temperatures is between $190-220°C$ for the nozzle and around $60°C$ for the bed temperature [35]. Finally, with the use of the igniters as seen in Section 2.4.3, there was a need for an igniter holder built into the 3D printed fuel grain structure. Due to the physical location of the igniter holder in the fuel grain, a 3D printed support is necessary and can be added into the print

file through Cura. Cura tells the printer to print this support with a much lower infill than the rest of the grain and not to fuse it with the rest of the grain. This makes it easy to pull off after the print is finished.

Solid Fuel Geometry

Outside of the composition of the fuel, the next most important part of the fuel grain is the shape, this is the case for both solid and hybrid rocket engines. The geometry of propellant grains have a big impact on the amount of thrust expected from a rocket and how that thrust will be delivered. The initial grain geometry will dictate the amount of surface area being burned at a given instant. As previously observed in equation 2.1.7 hybrid rocket chamber pressure increases with exposed burning surface area. Now referring to equation 2.1.3 using equation 2.1.2, it is easy to see that chamber pressure is directly proportional to thrust. Therefore, an increase in burning surface area will increase the amount of thrust produced by the hybrid rocket engine. This shows how important the initial grain and port geometry are to how much thrust will be produced at a given point throughout the engine's burn and will shape the overall burn profile. Typical burn profiles exhibit progressive, regressive, or neutral behaviors. Progressive profiles see an increase in thrust as burn time progresses, a regressive profile sees a decrease in thrust as burn time progresses, and a neutral profile sees thrust stay mostly constant throughout the burn time. Even though a neutral thrust profile is desirable because it does not change very much over time, it requires a very complex port geometry to keep the burning surface area constant with respect to time. Although, it is possible to create these complex geometries with a hybrid rocket engine because of FDM printing, this study will only focus on a single tubular core geometry due to its ease of design, and ease of comparison with solid rocket motors. Observation of various core geometries and their respective thrust profiles can be observed in Figure 15 [8].

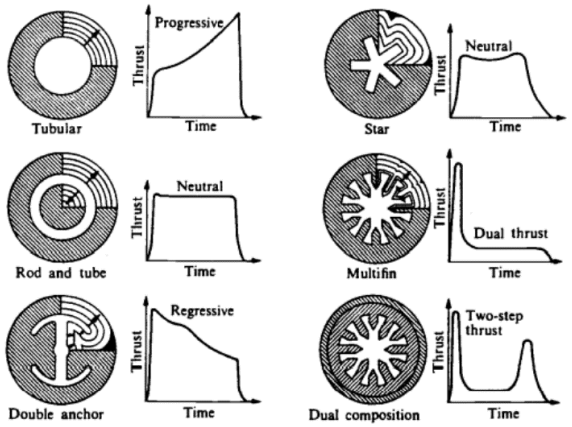

Figure 15: Grain Geometry Design and Typical Thrust Profiles [8]

2.6 Hybrid Rocket Mass Flow Rate

Even though the three types of chemical rockets are different compositionally, they all still depend on one component that accelerates the flow and helps produce thrust, the nozzle. As mentioned in Section 2.1 it is important for the nozzle to be sized properly for the local atmospheric conditions. If sized improperly the nozzle will underperform, as it is either expanding the flow from the rocket too much or too little leading to less thrust. Another important factor when it comes to nozzles is choking the flow at the throat. This means at the point with the smallest area, the throat, the flow needs to be travelling Mach 1, if the flow is not at Mach 1 there is a high chance for combustion instability or combustion to completely terminate. This is why it is crucial to have the nozzle sized properly. There are currently no studies focused on the effects varying the size of the nozzle has on the performance of a hybrid rocket engine.

2.7 Previous Works on Hybrid Rocket Engines

Even though the study of hybrid rockets has been limited until recently, there are some studies focused on hybrid rocket test stand design as well as certain studies focusing on ways in which some performance parameters could be improved.

Thomas et. al. designed a lab-scale hybrid rocket test stand using HTPB as their fuel and gaseous oxygen (GOX) as their oxidizer. The design of the stand included the use of structural t-slot aluminum and the use of two linear bearings. Chamber pressure ports were installed into the combustion chamber and thrust was measured by allowing the injector to press up against a load cell. In this study, the researchers found that the regression rate data from their tests coincided with other literature proving the stand would be an effective tool for evaluating novel hybrid rocket formulations [36]. The main issue with this test stand design is it is immobile. The design of the thrust stand can be seen in Figure 16.

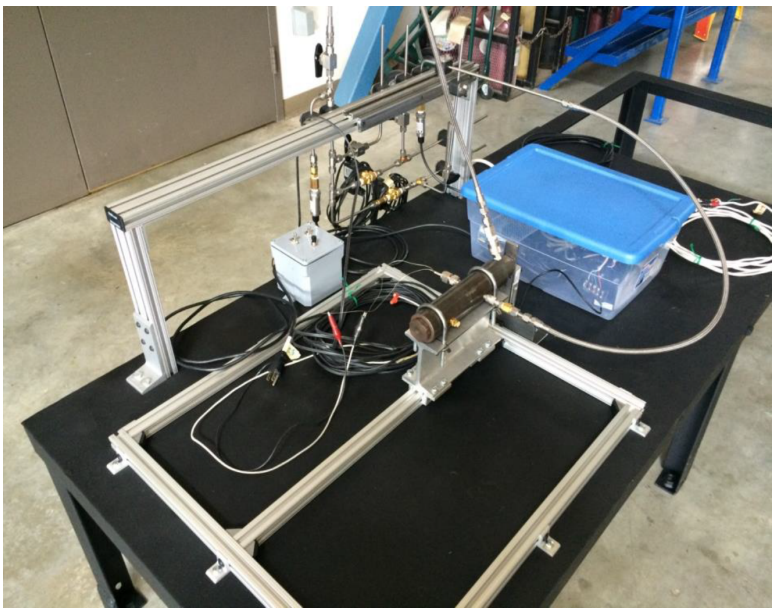

Figure 16: Hybrid Rocket Test Stand [36]

Bouziane et. al. also designed a lab scale hybrid rocket test stand, but this study used NOS as the oxidizer and paraffin wax as a fuel grain. The stand was designed to produce 225-lb (1-kN) of thrust and is controlled by a LabVIEW VI. The test stand proved effective [37]; however, the design of this stand does not allow for other sizes of combustion chambers or fuel grains.

Another study focusing on hybrid rocket test stand development was done by Summers. Even though this was part of the study, the main focus was developing a swirl injector system for the oxidizer [38]. This stand design is portable, but once again does not allow for various

sizes of combustion chambers or length of the fuel grain.

Mulato et. al. developed the entire hybrid rocket engine system as well as the test stand. This study, was successful in its objective of increasing performance parameters of oxidizer to fuel ratio and specific impulse [39].

Finally, Utley et. al. designed a portable, flexible use solid rocket test stand. The test stand was built for use in experimental motor research and development as well as for academic purposes. The design was successful in that the stand was able to collect data on specific impulse and total impulse within 1% of the commercially purchased solid rocket motor's manufacturers provided specifications [40].

The predominant nature of studies concerning hybrid rocket engine test stands have been focused on traditional types of fuel, like HTPB, and these test stands only allow for a singular sized combustion chamber. There is a lack of research into the design of a test stand which allows for various sizes of fuel grains, and various types of fuel grains, as well as a lack of research in the nozzle section of the hybrid rocket engine. With hybrid rocket engines coming to the front of the rocket industry, it seems fitting that a test stand be developed which can be easily adapted or modified to fit various oxidizers, oxidizer delivery systems, fuel grains, combustion chamber sizes, and nozzle sizes. Thus, the purpose of this study is to evaluate the design and construction of a portable, adaptable, and lab-scale hybrid rocket test stand as well as evaluating the performance of the hybrid rocket engine when the size of the nozzle is varied.

2.8 Theory of Analysis

This study primarily focuses on the design and evaluation of a horizontal hybrid rocket engine test stand. Which include analysis of the design, construction, implementation of instrumentation, evaluation of the test stand's performance, and determining whether the stand was able to make out changes in the rocket engine's performance. The other objective of the study is to evaluate the change in the engine's performance with various sizes

of nozzles. The performance of the hybrid rocket engine will be evaluated through various parameters. These parameters are peak thrust, average thrust, burn time, total and specific impulse. Tests were conducted using NOS as the engine's oxidizer, which had to flow through a pressure regulator, a solenoid valve, and an orifice plate before being injected into the combustion chamber. PLA was chosen as the fuel for the hybrid rocket engine. The dimensions of the PLA fuel grains are as follows: an outer diameter of 1.5-in, a total grain length of 3.5-in, and a tubular core size of 0.65-in. The various nozzle sizes used for the testing include a #13, #16, #19, and #25 size nozzle as well as 150-psi, 200-psi, and 250-psi for NOS feed pressures. Thrust will be recorded as a function of time for all tests.

CHAPTER III

TEST STAND DESIGN

3.1 Structural Design

The main objective of this study is to design and evaluate a hybrid rocket test stand. As discussed in the previous chapter, there are many ways in which a hybrid rocket test stand can be designed based on the desired size, data collection, and fuel or oxidizer selected for the stand. The designed test stand for this study attempts to implement the best qualities of some previous works while also including novel parts to enhance the performance of the overall stand and engine.

The base of the test stand is a rectangular steel table. The table has dimensions of 36-in wide, 48-in deep excluding the handle, and 42-in tall including the caster wheels. The table has 4 swivel casters with wheel locks, which allows the test stand to be mobile if desired. The wheel locks also prohibit the movement or rolling of the table during testing. The SOLIDWORKS design of the test stand can be seen in Figure 17.

The top and bottom of the table is made of 1/16-in thick steel sheet. These sheets are welded to 1.5-in square steel tubes which support provide the sheets with a solid structure. There are also three 1.5-in square steel tubes angled to support the legs of the table, these tubes are also welded to the legs. The table along with the casters is structurally sound and leaves no concern about the table's ability to withstand large amounts of thrust from the hybrid rocket engine.

Many of the test stand designs discussed in the Background and Theory chapter, were only able to accommodate a single engine casing size, or a single engine casing length. When

Figure 17: Table of the Test Stand

beginning the design process, it was of high importance to be able to change the casing size and casing length with ease. This single design parameter was the driving factor in all preliminary designs. The range of casing diameters was defined to be 1.5-in, 2-in, and 3-in, whereas, the range of casing lengths were 5-in to 20-in. In terms of solid rocket motors these sizes of casings include motors of class G (total impulse of 120-N-s) to class L (total impulse of 3600-N-s). The purpose of this design parameter would be to research new propellant formulations, and/or research the effect of increasing the size of the hybrid rocket engine for mission analysis purposes. While the larger hybrid rocket engines have a potential to reach a thrust level over 500-lb, this study focuses on 1.5-in diameter engine casings which will not be able to produce that amount of thrust. A maximum thrust of 100-lb was estimated for the tests in this study and was used to size the load cell.

While multiple design iterations were created, the process of incorporating both design constraints of casing length and casing size was increasingly difficult. One design idea was to mimic the design of Freeman [41], who compresses the motor casing using roller bearings which allows the casing to move forward but not jostle around during testing. The roller bearing configuration can be seen in Figure 18 [41].

While this design seemed enticing, especially for uses in solid rocket motors, there is a

Figure 18: Roller Bearing Configuration [41]

significant problem when it comes to hybrid rocket engines as the forward closure presses against the load cell. In a hybrid rocket engine, there should be minimal to no loading on the oxidizer feed system, but if this design were to be used the thrust would be directed through the injector fitting: increasing the chance of a failure. Another design idea focused on gripping the casing with routing clamps attached to linear bearings. The linear bearings allow the engine to slide, like the roller bearings. In this design the most forward linear bearing would press against the load cell, meaning the hybrid rocket engine would orient slightly above the load cell. This creates a slight moment arm and the thrust values output by load cell would have to be corrected.

The final design choice implements the use of the thrust ring on the outer surface of the casing. The casing is inserted into an aluminum plate with a hole large enough to fit the casing, but not large enough to allow the thrust ring to fit through. This aluminum plate is connected to two other aluminum plates: one supports the forward end of the casting, and the other presses against the load cell. All three plates, 4-in by 4-in by 1/8-in, are

connected with the use of four 1/2-20 threaded rods that are 2-ft in length and secured with the appropriately sized hex nuts. The most forward and aft plates are connected to a T-slotted framing structural L bracket which are then mounted to T-slot linear bearings. The final design is shown in the following Figure.

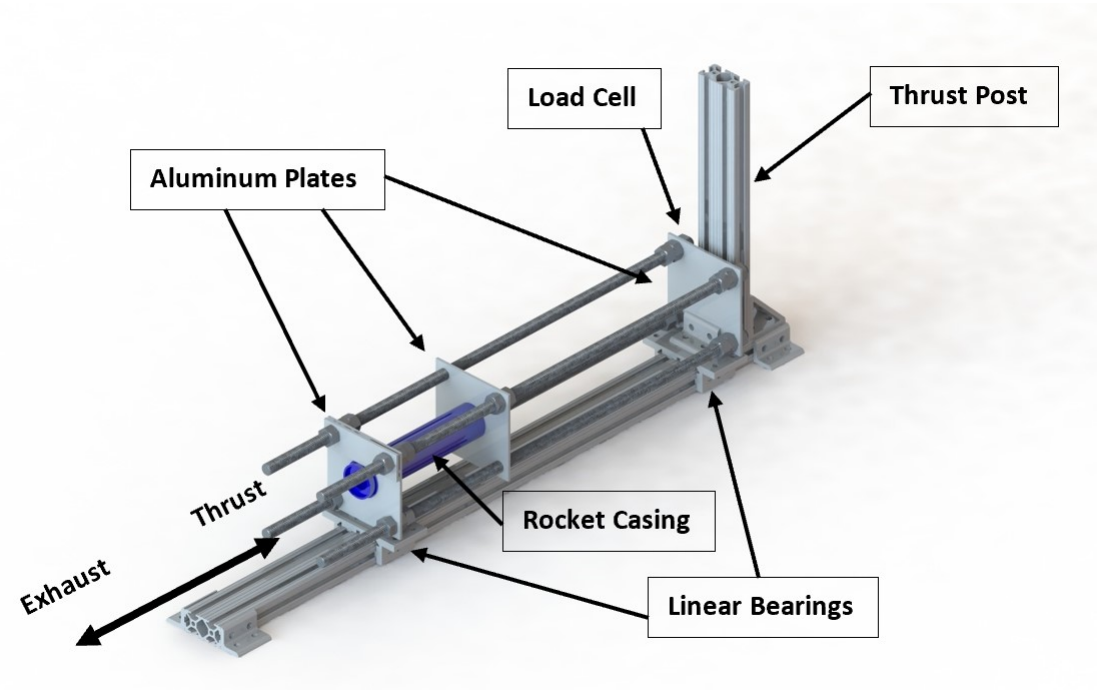

Figure 19: Test Stand Structure

Figure 19 only shows the structure of the stand including the casing; however, it does not display the oxidizer delivery system. This will be shown and described in the following section. The base of the design is the use of 1-in double T-slot aluminum framing. The horizontal guide rail, which houses the linear bearings of the test stand, is 32-in in length to accommodate long engine casings. The vertical thrust post, which braces against thrust force created by the engine and is 12-in long, is supported by an open extended gusset bracket opposite of the thrust load. The front side of the thrust post contains the load cell. The Futek LLB400 500-lb capacity load cell has three #6-32 threaded holes. The load cell is connected to a 1/8-in thick aluminum plate using the holes. The adapter plate is then bolted to the thrust post and can be moved up or down depending on the size of the engine

to get the line of thrust directly in the center of the load cell. Figure 20 shows how the load cell and adapter plate connected to the thrust post.

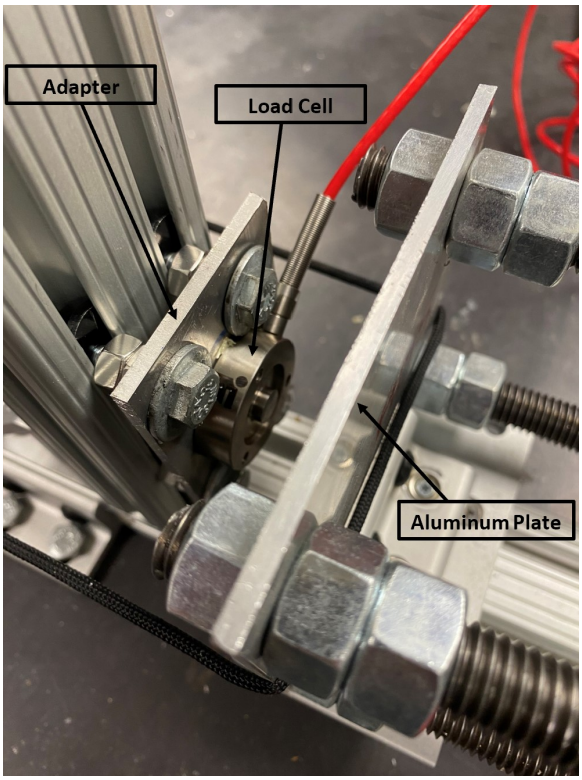

Figure 20: Load Cell Integration

The test stand is mounted to the rolling table with the use of T-slot corner brackets and 1/4-20 fasteners which are widely used for T-slot structural framing. There are two corner brackets on each side of the horizontal guide rail at the forward and aft ends of the test stand. The final main component of the test stand is the thrust ring holder. Even though the engine casing is placed through the aft most aluminum plate and the thrust of the engine forces the engine forward, if a catastrophic failure were to occur and the engine casing separated from the oxidizer delivery system, the engine casing could be displaced from the test stand and cause harm to the surrounding environment. To prevent this from happening, a thrust ring holder was designed. The thrust ring holder and the aft most aluminum plate hold the thrust ring in place, not allowing any movement of the engine casing. The thrust ring holder is 4-in by 1 1/4-in by 1/8-in and made of aluminum. It, like the 4-in by 4-in aluminum

plates is placed on the 1/2-in threaded rods and tightened with the appropriately sized nuts to hold it in place during testing.

3.2 Oxidizer Delivery System Design

An oxidizer delivery system was designed to safely introduce the oxidizer to the solid fuel grain and maximize the performance of the engine. The delivery system includes the small 10-lb testing bottle, bottle mounting clamps, fittings, steel braided hoses, a pressure regulator, solenoid valve, orifice plate, and forward closure (injector).

The small 10-lb has a 6-Army Navy (AN) male fitting and a pressure gauge which displays the static temperature inside the bottle. Even though the bottle has this pressure gauge, NOS has a great property: self-pressurization. This means the pressure of NOS in a contained cylinder is highly dependent on the ambient pressure. Table 4 presents the pressure of NOS at certain temperatures [42].

Bottle Temperature (°F)	Bottle Pressure (psi)
32	460
40	520
50	590
60	675
70	760
80	865

Table 4: NOS Pressure Based on Bottle Temperature [42]

The table shows at room temperature the bottle pressure can be expected to be near 800-psi. This is consistent with the pressure gauge display threaded onto the small 10-lb testing bottle. The next part of the oxidizer delivery system design is the bottle mounting clamps. The bottle mounting clamps are thin, flexible sheets of metal which wrap around the bottle and hold it in place during testing. The clamps are mounted to the table, the bottle

slides in and is then tightened down using wing nuts attached to the clamps. The mounted small bottle can be seen in Figure 30. After, the bottle placement and mounting structure was decided upon, the design of the rest of the oxidizer delivery system ensued. To get the NOS from the bottle, mounted under the top of the table, into the combustion chamber a 6-ft stainless steel braided hose was used. This hose, though flexible, can withstand up to 1200-psi and is extremely durable. The hose has 6-AN female fittings, making it compatible with the small 10-lb testing bottle.

While the testing bottle and the hose have 6-AN fittings the rest of the oxidizer delivery system has 1/4-in NPT style fittings. To transition from the AN to NPT style fittings, a male 6-AN to female 1/4-in NPT adapter was used. This type of adapter is commonly used in automotive racing cars, it is made of plated steel and will be able to handle the temperatures and pressures exerted onto it by the NOS. Now that the oxidizer delivery system has transitioned from AN to NPT fittings the next step in the design process was to determine how to regulate the mass flow rate of oxidizer entering the combustion chamber. There are two possible ways of doing this. The first is to keep the feed pressure constant (at the tank pressure) and create orifice plates with varying sizes of holes. Or, the second option, varying the feed pressure using a pressure regulator and using a single orifice plate. Either option essentially performs the same task; however, the use of a pressure regulator allows the test stand operator to adjust the mass flow rate of oxidizer more easily by changing the outlet pressure of the regulator.

The final choice in the mass flow regulation portion of the oxidizer delivery system, was to use a pressure regulator and a single orifice plate. Once this choice had been made, the process of determining the proper pressure regulator and sizing of the orifice plate began. Many pressure regulators on the market are not made for the supply pressure coming out of the small 10-lb testing bottle. Typical pressure regulators can handle a range from 0-psi to 200-psi supply pressure and have an output pressure range of 50-psi to 150-psi. The pressure regulator for this system would be required to handle a supply pressure of at least 1000-

psi and have an outlet pressure minimum of 200-psi. Thus, the Pressure Pro II regulator was selected. The Pressure Pro II can handle a supply pressure up to 4500-psi and has an adjustable output pressure of 200-psi to 1100-psi. Another plus in getting this style of regulator are the inlet and outlet connections are 1/4-NPT; which means there will be no need for additional fittings or sizing adapters.

For this mass flow rate regulation setup to work, an orifice plate was also needed. The plate selected is 6-in by 6-in by 1/4-in and made of 304 Stainless Steel. This material will be able to handle the large pressure and velocities imposed upon it by the flow of NOS. Because the plate is not threaded, two high pressure pipe flanges and adapters made of 304 Stainless Steel were used. The pipe flanges have a thread of 1/2-NPT whereas the rest of the oxidizer delivery system is made up of mostly 1/4-NPT, therefore the 1/4-NPT to 1/2-NPT adapters are needed. Both the pipe flanges and the adapters can handle the pressure from the NOS. The orifice plate in this feed system is meant to choke the flow, also known as forcing the flow to be Mach 1 inside the opening in the plate. For this to occur an extensive analysis was done to determine the diameter of the orifice in the plate.

The first step in the analysis was to make an arbitrary guess as to what the orifice plate hole diameter should be. This was initially chosen to be 1/4-in. The next step would be to find the mass flow rate at various pressures supplied from the pressure regulator. The relation used for this analysis is the Mass Flow Parameter and can be seen in the following equation.

$$MFP = \frac{\dot{m}}{A}\frac{\sqrt{T_t}}{P_t} \tag{3.2.1}$$

To solve for mass flow rate, Equation 3.2.1 is rearranged for mass flow rate. Where T_t is the ambient temperature in Rankine and was assumed to be 532 R, P_t is varied from 200-psi to 400-psi by increments of 50-psi, A is the area of the hole in the plate, and MFP is found by using the Gas Tables program in the free AEDsys software. To get MFP from the Gas Tables program, the ratio of specific heats, γ, and the molecular weight of the gas

must be known. It is also assumed, when using this program, that the flow of NOS will be isentropic. γ for NOS was assumed to be 1.4, and the molecular weight of NOS was found to be 44-g/mol [43]. Once this information is input to the Gas Tables, the output MFP is equal to 0.655-(lbm-$R^{1/2}$)/(s-lbf). Once all of the necessary information was found, an iterative process began calculating the mass flow rate of NOS at the various feed pressures mentioned above.

After this iterative analysis was complete, the hole diameter of the orifice plate could then be fine-tuned. This involved solving for the chamber pressure at the various feed pressures, to ensure the chamber pressure was at least 20% less than that of the feed pressure [44]. Although, the arbitrary guess of 1/4-in diameter for the hole was a good initial estimate, it was determined the hole diameter should be 0.24-in to obtain a proper chamber pressure. The final step in the design process of the orifice plate was to determine how much the hole in the orifice plate should be tapered. If the orifice plate was not tapered, the discharge coefficient would be very low. The discharge coefficient is used to calculate the amount of loss a flow sees through an orifice. While an orifice has a low discharge coefficient (meaning large losses); a tapered orifice, or Venturi nozzle, has a high discharge coefficient (meaning low losses). The discharge coefficient is a function of the ratio of orifice diameter to pipe diameter ($\beta = d/D$) and the Reynolds Number [45]. By finding the Reynolds Number and using the proper equation from *Munson, Young and Okiishi's Fundamentals of Fluid Mechanics* the discharge coefficient was found to be 0.975 with a tapering angle of 45°. Additional holes were added in the orifice plate to allow the pipe flanges to be bolted together with the plate in between the two. A cross-section view drawing of the orifice and orifice plate can be seen in Figure 21.

A solenoid valve was placed in between the pressure regulator and orifice plate. The chosen solenoid for the oxidizer delivery system is a Burkert 6027 solenoid valve. This solenoid can handle pressures up to 1450-psi (100-bar) and a range of temperatures from 14°F through 284°. Extra analysis was done to ensure the solenoid did not choke the flow

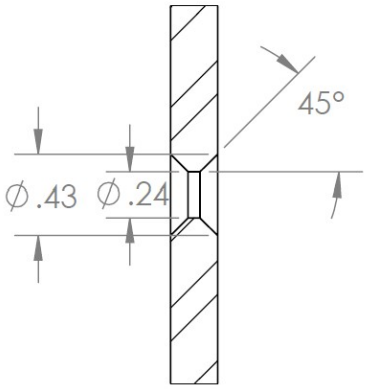

Figure 21: Section View of Finalized Orifice Plate

and restrict the mass flow rate because that is the purpose of the orifice plate. Hybrid rocket engines generally have throttling capabilities, in that their oxidizer mass flow rate can be changed, but this solenoid does not have the ability to throttle because it has two steps, on or off. The solenoid chosen for this study has female 1/4-NPT fittings on the inlet and outlet side. The inlet side is directly connected to the outlet of the pressure regulator, and the outlet side is connected to the pipe flange of the orifice plate by a 3-in brass pipe. As will be described in the next section, the solenoid is electronically controlled and will be opened and closed at set times to know the exact mass flow rate of the NOS. A rendering of the oxidizer feed system can be seen in Figure 22.

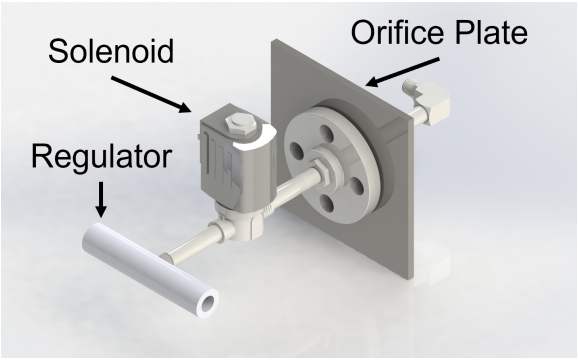

Figure 22: Oxidizer Feed System Rendering

3.3 Measurement Systems Design

The measurement system is split into the user interface, a measurement input, and two control outputs. A diagram of how the three groups are connected can be seen in the following figure.

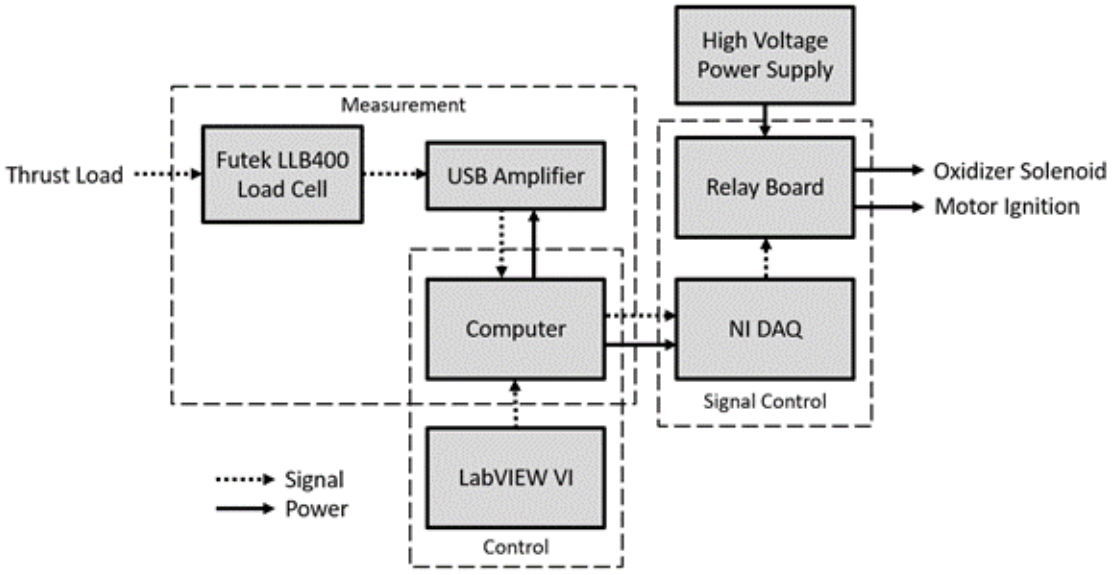

Figure 23: Measurement System Power and Signal Path

A LabVIEW VI was developed to integrate the Futek loadcell, solenoid flow control, and ignition system into a single user interface. This was done using a Message Queue Handling architecture, which allows for parallel processes to take place in independent loops. The control loops are connected to an event handling loop, where the user interface sends commands. This results in inherently modular code that can be easily modified to allow for both physical and software functionality to be added. Figure 24 shows the data collections module.

The Futek LLB400 allows for high resolution and sampling rate data collection, which can be configured for each test. For system controls, a National Instruments USB-6211 DAQ board is used for two signal outputs. These two signals go to two high-voltage power relays on an eight-relay board. When pulled high, these relays complete the 24-volt DC circuit for

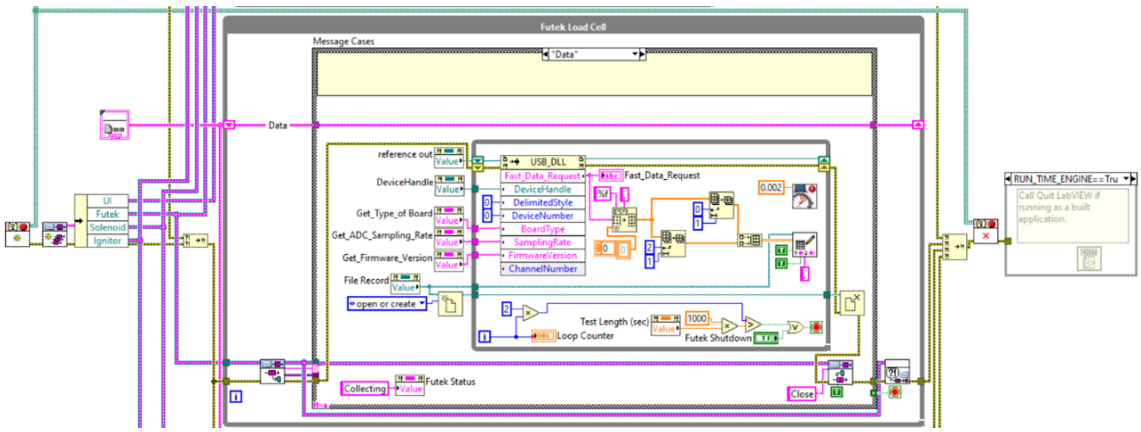

Figure 24: LabVIEW Data Collection Module

either the oxidizer solenoid or motor ignition respectively. The duration and timing offsets of these events are inputs within the LabVIEW user interface, allowing for sub-second tuning of events. The Futek load cell and NI DAQ are both powered from USB 5-volt power, while the high-voltage systems are powered by a National Instruments PS-15 Power Supply.

3.4 Pre-Load Design

The final design component of the test stand is a pre-loading pulley system. Pre-loading the load cell is intended to aid in calibration of the system and to improve data quality by damping any movements of the combustion chamber during testing.

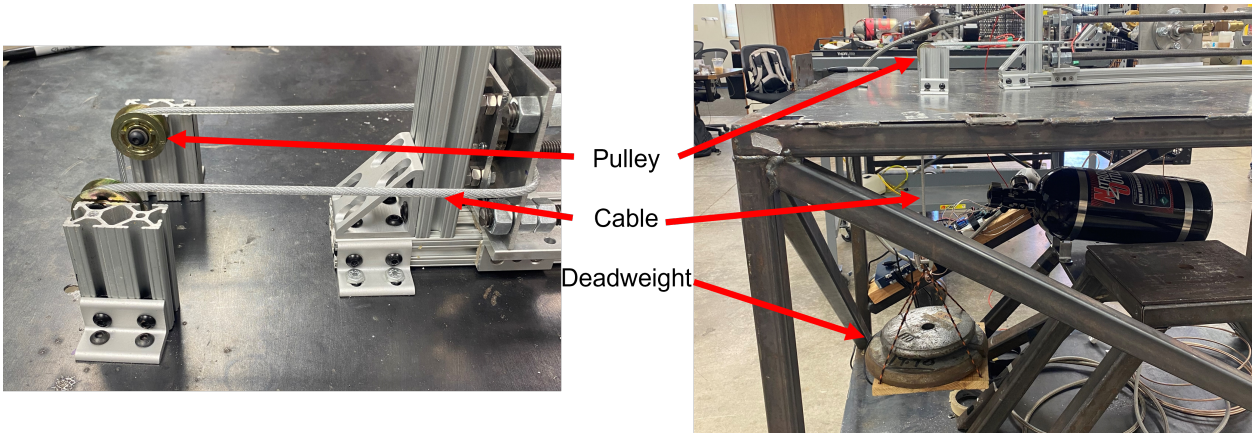

Figure 25: Pre-Load Design

The pre-load design was done using a cable-pulley system with dead weight handing under the test stand tabletop surface. The cable wraps around the forward most aluminum plate and pulls the linear bearings, combustion chamber, and oxidizer feed system forward. Calibration weights of 3.5-lb, 4-lb, and 4.5-lb were used on the pre-load system to create a calibration curve for the load cell to determine actual thrust produced from tests. The weights produced a curve which was then applied to all data points output by the load cell during the testing phase of this study. The pre-load system can be seen in Figure 25.

CHAPTER IV

EXPERIMENTAL SETUP AND PROCEDURES

4.1 Hybrid Engine Propellant Storage

The facility in which this study was performed is the Oklahoma State University Richmond Hill Research Laboratory. All ingredients for engine fabrication, testing, and storage are located within this facility. All hybrid rocket engine related items are kept in a limited access and secure room within the facility that prevents unauthorized personnel to be in contact with items related to hybrid rocket engine manufacturing and testing. All engine ingredients are stored in their proper places. PLA that is used to print the hybrid rocket solid fuel grain is stored on or near its respective 3D printer. The NOS is stored in a thick steel 50-lb bottle in a safe secure space with proper labeling.

4.2 Solid Fuel Manufacturing

4.2.1 Solid Fuel Design

To test an engine on the hybrid rocket test stand, the first step of the process is to design and manufacture the solid fuel grain. As mentioned previously, the solid fuel grain is composed of 3D printed PLA. The 3D printer used for this study is a Creality Ender 5, which has a relatively large build area (9 x 9 x 12-in) and makes good quality prints. The PLA used for this study is the White Build Series PLA 0.07-in from MatterHackers. This PLA was chosen because of its consistency when printed, the price of the filament, and its widespread use makes it easy to obtain. All solid fuel grain prints followed the instructions of the Ender 5

manual [46].

Before the fuel grains could be printed on the Ender 5, they needed to be designed using a CAD software. For this study SOLIDWORKS was used to not only design the test stand prior to construction, but it was also used to design the solid fuel grains. As mentioned before, the port geometry of the fuel grain is a Bates grain, meaning a straight hole through the center of the grain. Initial designs for the fuel grain were 1.5-in in diameter, had a length of 3.5 inches, and a port geometry size of 0.65 in, as seen in Figure 26.

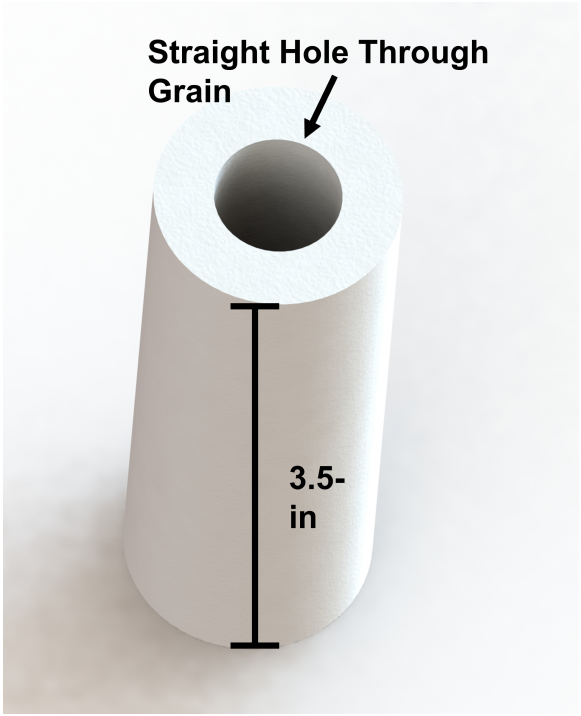

Figure 26: Initial Fuel Grain Design

Although this core geometry works for solid rocket motors, a straight hole through the center of the hybrid grain makes ignition and the combustion process difficult. This is due to the fact that the solenoid valve is opened, and the NOS begins to flow before the ignition process begins. Preliminary tests showed immense difficulty with keeping the igniter inside the combustion chamber while the NOS was flowing. Thus, it was necessary to make some design adjustments to the fuel grain. All the initial dimensions stayed the same; however, an igniter holder was added into the final design. This igniter holder was designed with 6

fins to give the holder some structure as well as to promote initial mixing and combustion of the PLA with NOS that would then spread to the rest of the fuel grain. The igniter holder itself acts as a "bucket" with a small hole in the bottom to allow the wire leads to come out of the engine and attach to their proper alligator clips. The igniter holder can be seen in Figure 27.

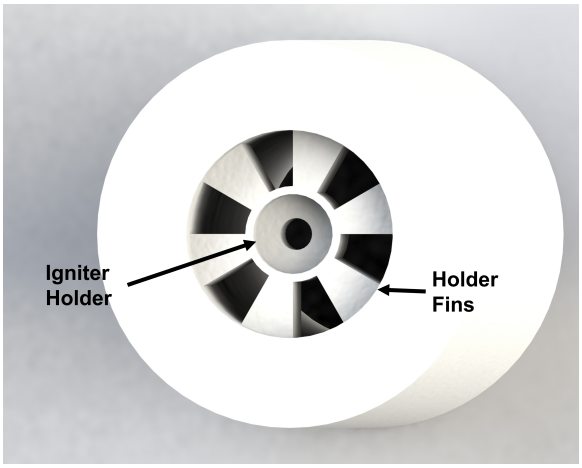

Figure 27: Fuel Grain with Igniter Holder

Once this fuel grain was designed, additional preliminary testing took place to prove the effectiveness of the igniter holder. These tests confirm the igniter holder design validity.

4.2.2 Solid Fuel Slicing

Once the fuel grain has been designed using the CAD software, it needs to be prepared for the printer. This is done by saving the SOLIDWORKS part file as an STL file and opened in the slicing software Cura. As mentioned previously, within the slicing software the designer can change many variables. For this study the infill percent of the fuel grains was kept constant at 50%, this means inside the solid exterior walls of the fuel grain 50% of the volume will be filled with PLA. In Cura, the pattern in which the infill is printed can also be changed. There are quite a few options for this; however, All3DP [47] has suggestions for the infill pattern depending on the use of the 3D print. For this study, the recommended cubic infill pattern is chosen because of its common applications in functional 3D prints. It is also Cura's first

suggestion when the infill percentage is at or above 50%. The next variable in Cura is the nozzle and heated bed temperatures. For PLA the suggested nozzle temperature is between $190 - 220°C$ and can be finely adjusted depending on the overall print environment. For the Ender 5 printer there is not an enclosure surrounding the printer, meaning if the printer is contained in a colder environment the nozzle temperature should be on the higher end of the suggested range. For this study it was determined the nozzle temperature should be $212°C$ for the best results. The Ender 5 also has a heated bed, which helps with bed adhesion, prevents print warping, and assists in print removal. For this study the bed temperature was set to $60°C$, at this temperature the base layers of the print do not come off the heated bed and warp the print as they stay adhered to the bed throughout the entirety of the print. After the print is complete and the bed cools off, the bottom layers retract just enough for the print to be removed from the bed cleanly and easily. Another variable changed in this study is the print speed. The suggested print speed in Cura for a print made on the Ender 5 is 80-mm/s, increasing this speed means the print might be of a lower quality; however, it will also take less time. Decreasing the print speed would have the inverse effect of increasing the print speed. Although the suggested print speed for the Ender 5 by Cura is 80-mm/s, the print speed for this study was set to 70-mm/s as it creates a higher quality print and does not extend the print time to excessive levels. With the original fuel grain, no support was necessary because the print was essentially a vertical cylinder, but with the inclusion of the igniter holder, the addition of a print support was deemed necessary. To create a support in Cura, all that is needed is to check a box and it automatically inserts a support in the print. The last setting adjusted in Cura, was the use of a brim. A brim is a type of build plate adhesion measure. It aids the first layer of the print in adhering to the bed throughout the printing process.

Once all the settings have been set to the desired values, it is time to slice the print and get it onto a SD card. In Cura, after the print is sliced, the print time will show up along with the ability to save the sliced gcode file to a SD card, this can be seen in Figure 28. The

other noticeable portion of this figure is the weight of the grain. Each grain printed used 54 grams of filament, but this includes the brim and the support. The actual weight of the grain itself is 51 grams. This value is important for understanding parameters like fuel mass flow rate, burn rate, and thrust. When ready the SD card is removed from the computer and is ready for the printing process to begin.

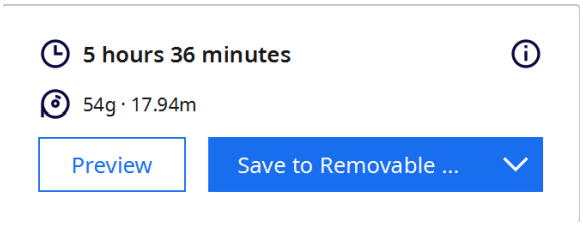

Figure 28: Cura Print Time

4.2.3 Solid Fuel 3D Printing

After all the design and slicing has been completed the print can begin. The Ender 5 must be turned on and the SD card is then inserted into the proper slot. Then whoever is running the printer must go to the Ender 5 control panel and initialize the SD card. Initializing the SD card allows the user to enter the SD card files from the printer. Then the user will select the desired gcode file to be printed, and the print begins. When a print is stared on the Ender 5, the bed heats to the desired temperature followed by the nozzle and can be monitored on the control panel. Following the completion of the heating process the Ender 5 brings the bed and the nozzle to the home position to ensure proper location of the nozzle and bed. Finally, the actual print ensues. Some of the main issues that can be encountered when printing with the Ender 5 are the deterioration of the nozzle and the lack of automated bed leveling which can change over time. After many prints the steel nozzles can begin to perform poorly, some of these symptoms include skipping print layers, stringy material being extruded from the nozzle, and inconsistent extrusion patterns. This problem is easily fixed by changing out the nozzle following the Ender 5 manual [46]. Despite not having an automated bed leveling system, the Ender 5 does have the ability to manually

level the bed. The printer has four knobs that control the bed in each corner and can be adjusted up or down by rotating the knob clockwise or counterclockwise depending on the desired height of the bed. Throughout the process of printing the grains for this study, the nozzle was changed once despite showing no obvious signs of deterioration. This was done as a preventative measure. Also, the bed was re-leveled once again as a preventative measure to ensure no problems with the printed fuel grains. All the fuel grain prints came out just as designed, and the supports that were added in during the slicing process were removed easily without impacting the grain in any way.

4.3 Fluid Oxidizer Preparation

4.3.1 Large 50 lb Bottle

The large 50-lb bottle of NOS was obtained, the bottle is safe to store in an open area away from high temperature and flames. This size bottle was chosen because it allows for up to 5 full refills of the 10-lb bottle and comes at a good price. These bottles are used throughout the automotive industry to refill smaller bottles that go into vehicles. While these bottles contain a large amount of NOS, they cannot be legally refilled. Once they are empty, they are replaced by the distributor and the used bottles are properly recycled. Although the most common way of storing these bottles is upright, it was determined that a bottle stand was necessary. This bottle stand aids in refilling the small 10-lb bottle through gravity, but it also provides the large bottle with a larger and more supportive base than the actual base of the bottle. The large mother bottle is inverted and threaded into the stand to ensure no tipping or leaning of a large bottle. Additionally, there is a wall mount with straps wrapping around the bottle to keep the bottle stable in the event someone bumps into it or another extenuating circumstance occurs. The other important piece of the mother bottle is the heating blanket. The heating blanket increases the temperature of the bottle; therefore, increasing the temperature of the NOS. The heating blanket is used when the refill process

is ongoing and by increasing the temperature the pressure is increased and the NOS flows out of the large 50-lb bottle into the refill station.

4.3.2 NOS Refill Station

For ease of mobility as well as being able to attach a NOS bottle to the test stand a small 10-lb testing bottle was selected, described in Section 2.5.1. Although, this smaller bottle is sized properly for the test stand, the ability to transfer the NOS from the large 50-lb bottle to the smaller 10-lb bottle became an issue. There are two ways in which the NOS can be transferred: gravity fed, and pump fed. For the gravity feed system to work many additional parts and pieces would be needed to make sure the fluid would be flowing from the large bottle into the smaller bottle. With the pump feed system, the larger 50-lb bottle is attached to a pump which pulls the NOS out and pushes it into the smaller 10-lb bottle. The clear choice for safely refilling the small 10-lb bottle was the pump fed type. The NOS pump filling station was selected and can be seen in Figure 29 [48]. The filling station comes with a heavy-duty automotive NOS pump, a NOS filter, a 1/4 turn valve, and all necessary hoses and attachments to complete a refill. Along with the station a compressed air pump was used. This pump is necessary if the filling process begins to slow down before the bottle is full and aids in the process of refilling.

Figure 29: Nitrous Outlet Pump Station and Scale [48]

As can be seen in the previous Figure, this pump fed system comes with all necessary fittings, hoses, and scales to complete a proper fill. With the purchase of the Nitrous Outlet

pump refill station also came an instruction manual providing safe operating procedures. These procedures are as follows:

1. Turn on the weight scale and let it zero out.

2. While the scale starts up make sure your 1/4 turn valve is closed and open the mother bottle.

3. Set your small nitrous bottle on the scale and see how much it weighs with the amount of nitrous that is in it.

4. Attach your fill hose to the small bottle nipple and tighten. Slowly open your 1/4 turn valve. This will push all the air to your bottle nipple.

5. Now crack the fill hose at the bottle nipple to bleed the air out of the system to ensure a proper fill. You will know all the air is bled out of the system when there is a solid plume of nitrous coming out of the fill hose end.

6. The side of the bottle will have the weight of the bottle only, maximum weight of the gas, and a total weight of the bottle and gas. Take the number from Step 2 and subtract if from the total weight of the bottle and gas.

7. Now that you know how much you need to fill, and the air is purged out of the system you are ready to fill. Zero your scale and open the bottle valve slowly till you hear the nitrous flowing steadily in the bottle and continue to open till it is wide open. If your bottle is cold, you may not have to run the nitrous pump, but if your bottle is room temp or hotter turn the air valve and the pump will start filling. Close the air valve when you get close to your target weight. Shut off the 1/4 turn valve and close your bottle valve. Crack your fill line so you can purge the line and remove it.

8. Verify that you have a complete fill, take the bottle off the scale and zero it out. Once it is zeroed out, place the bottle back on the scale to get a complete weight of the

bottle and gas together. If it is close to 23.9-lbs then you have successfully completed a proper fill.

4.3.3 NOS Delivery System

After the small 10-lb testing bottle has been refilled, it is time to mount it to the test stand and connect the oxidizer delivery system to the bottle. The small test bottle mounted to the test stand can be seen in Figure 30.

Figure 30: Small Bottle Mounted to the Test Stand

Connecting the bottle to the oxidizer delivery system is done by using the long 6 ft hose and threading the female end of the hose onto the male bottle fitting. A 3/4-inch wrench is used to ensure a tight seal on this thread. While the rest of the oxidizer system stays intact throughout all tests, it is important to check each fitting for leaks or loose connections. This pre-test check is also done with the 3/4-inch wrench. When each fitting is properly tightened, the rest of the oxidizer delivery system is prepared. This preparation includes

setting the pressure regulator to the desired outlet pressure, ensuring the solenoid valve is in the off position, the orifice valve bolts are tightened, and the male injector fitting must have fresh thread tape applied. These steps must be completed before each test to ensure no malfunction with the oxidizer delivery system.

4.4 Hybrid Engine Motor Testing

4.4.1 Solid Fuel Test Preparation

Once the solid fuel grains have been designed, sliced, and printed, the grains need to be prepared for testing. Each grain is inserted into a phenolic liner. The purpose of the liner is to thermally protect the casing from reaching elevated temperatures and causing failure. The phenolic liner is then cut to size, and a solid fuel fit check is completed. The fit check consists of assembling the aluminum casing and snap ring configuration shown in Figures 31 and 32. Figure 31 shows the exploded view of the assembly and Figure 32 shows a section view of the way the components fit inside the aluminum casing.

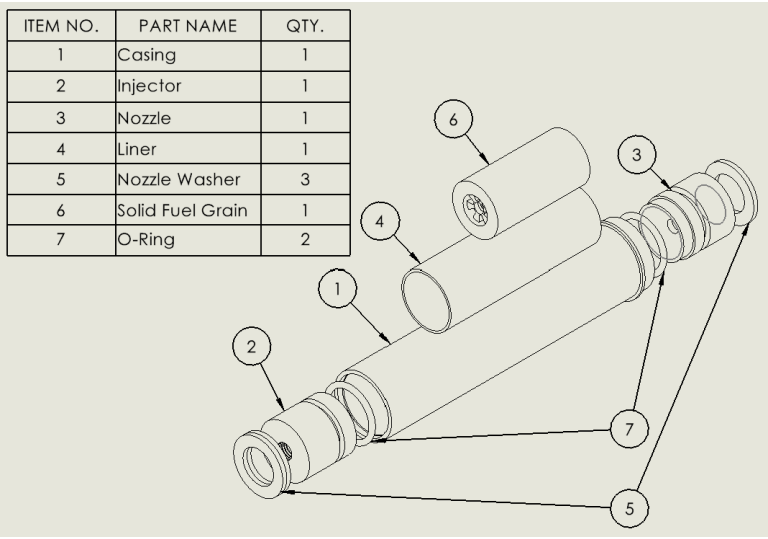

Figure 31: Solid Fuel Assembly Exploded View

In this assembly, the forward closure has a threaded end which allows the injector fitting of the oxidizer delivery system to be connected to the fuel grain and combustion chamber.

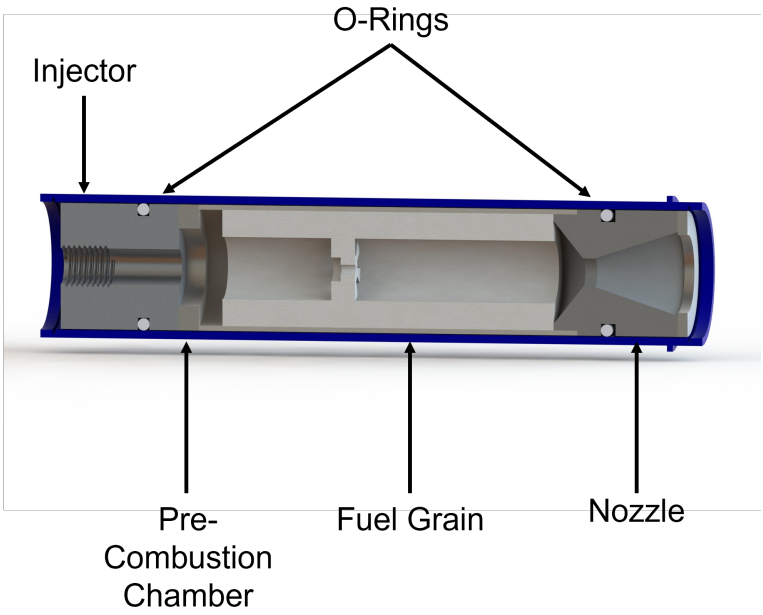

Figure 32: Section View of the Solid Fuel Assembly

The forward closure is sealed with the use of an O-ring and a snap ring is placed forward of the closure to complete the front section of the assembly. Going aft of the forward closure additional nozzle washers are used as a pre-combustion chamber to allow for better mixing of the NOS. After the pre-combustion chamber, the fuel grain is inside of the appropriately sized liner, and interfaces directly with the converging-diverging nozzle. The nozzle is also sealed with an O-ring and is pressed against a nozzle washer to distribute the forces from the nozzle. Aft of the nozzle washer is another snap ring to complete the aft section of the assembly.

After the fit check is complete the outer surface of the solid fuel grain is coated in high strength glue and is inserted back into the liner. The grain is glued to the liner to prevent any movement during testing. The glue must be left to dry for at least 8 hours to allow for adequate drying. Once the glue has dried the solid fuel assembly can be fully prepared for testing. The final assembly begins by coating the outside of the liner with a thin layer of silicone grease. The O-rings are then greased and placed within the proper grooves of the nozzle and forward closure. The aft end of the liner is pressed onto the converging side of

the graphite nozzle. The nozzle and liner, now housing the solid propellant grain, can now be slid into the aluminum casing making sure the diverging section of the nozzle is facing the aft end of the casing when fully installed. A nozzle washer is then placed on the exit face of the nozzle, and the forward closure is slid into the casing through the forward side with the injector side being flush to the face of the liner. Snap rings are then placed into the snap ring grooves on the forward and aft sides of the casing.

4.5 Test Procedures

All testing is conducted behind the north loading dock at the Richmond Hills Research Complex. The testing environment allows for compliance with recommended safety precautions regarding standoff distances, hearing protection, and accessible fire extinguishers.

Installed Total Impulse (N-s)	Equivalent High Power Motor Type	Min. Diameter of Cleared Area (ft.)	Min. Personnel Distance (ft.)
0-320.00	H or smaller	50	100
320.01-640.00	I	50	100
640.01-1280.00	J	50	100
1280.01-2560.00	K	75	200
2560.01-5120.00	L	100	300
5120.01-10240.00	M	125	500
10240.01-20480.00	N	125	1000
20480.01-40960.00	O	125	1500

Table 5: National Association of Rocketry Standoff Distances for High Powered Motor Testing [49]

Although the system is a hybrid rocket, the safety standards for solid rocket motors are followed for this study. National Association of Rocketry high powered launch safe standoff

distances can be observed in Table 5 [49]. Testing procedures for hybrid rocket engine testing are as follows:

1. Insert the igniter leads through the forward closure and through the nozzle until the igniter is seated in the igniter holder.
2. Use the aft aluminum plates to slide the combustion chamber into place.
3. Thread the combustion chamber onto the male fitting of the oxidizer feed system.
4. Apply 10-lb of pre-load to test stand load cell.
5. Tighten the thrust ring holder plate to the aft-most aluminum plate.
6. Connect the Futek usb and DAQ usb to the testing laptop and plug in the extension cord for the power supply.
7. Launch the LabVIEW VI and type in the load cell serial number, sampling rate, and choose a data output file location.
8. In the VI set the total test length, the oxidizer delay, the igniter delay, and the oxidizer duration.
9. Ensure the solenoid valve is closed and open the testing bottle valve, NOS can be heard going to the solenoid.
10. After the bottle is open, set the pressure regulator to the desired pressure with a 3/16-in Allen wrench.
11. Take the installed igniter, strip the leads and connect them to the test stand alligator clips. Be sure to touch alligator clips together before connecting the igniter leads to ensure that no voltage is being sent through the igniter during installation.
12. On the testing laptop, run the code. This will not start the test, but it allows the load cell to be configured.

13. Once the system status on the VI says "Configured", a countdown from 5 may begin and the "Start Test" button can be clicked.

14. Once the test has been completed, close the testing bottle and bleed the braided hose to ensure no ghost flames inside the combustion chamber.

15. Allow combustion chamber to cool to the touch before removing chamber from the test stand by loosening the bolts on the thrust ring holder, and begin disposal of single-use parts.

An image of engine testing in progress can be seen in the following figure.

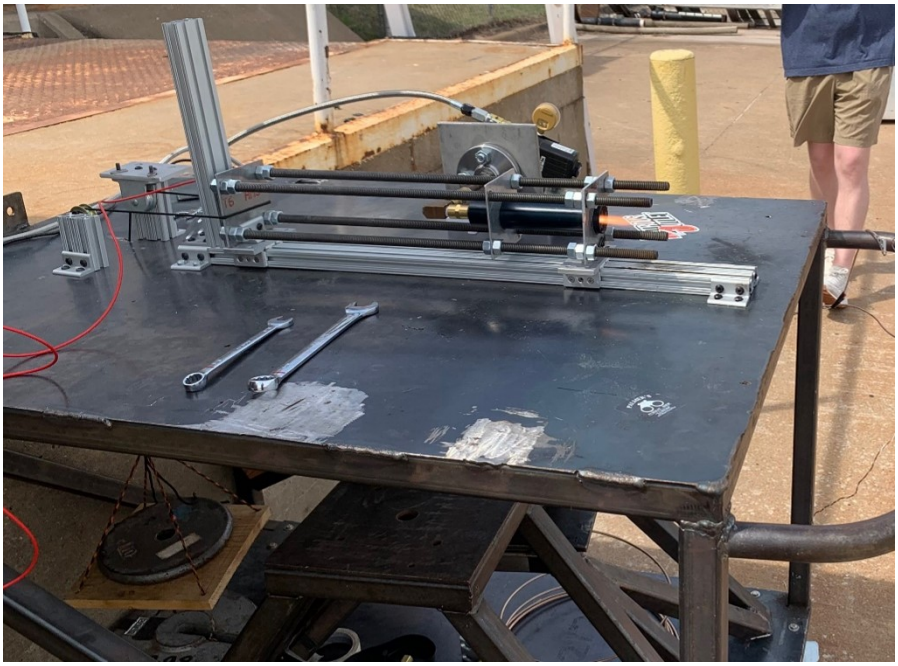

Figure 33: Hybrid Rocket Engine Test

CHAPTER V

RESULTS

5.1 Analytical Estimation of Performance

Before testing was conducted, an analytical estimation of hybrid rocket thrust was created. This analysis can be found in Appendix 1 and uses the mass flow rate of NOS summed with an estimation of PLA mass flow rate to find a total mass flow rate out of the engine. With this total, another mass flow parameter calculation was completed. In this second calculation, the chamber pressure and combustion temperature were estimated to match the mass flow rate from the first calculation. Once the mass flow rates matched, the temperature and pressure were then used in an extensive thrust estimation.

To estimate the thrust produced by the hybrid rocket engine, a NASA CEA simulation was completed to aid the process [50]. The input values in the CEA are chamber pressures, fuel, oxidizer, and nozzle expansion ratio. Although the CEA has NOS as an oxidizer choice, it does not have PLA as a fuel option. Therefore, when running the CEA acetic acid was chosen as the fuel because it is the most similar option molecularly to PLA, missing a single carbon atom. The output CEA file provides an exit Mach value, ratio of specific heat value, and the specific heat value of the products.

After running the CEA, isentropic pressure and temperature ratios were calculated and used to find the static temperature and pressure values. The static temperature value was then used to find the exit velocity of the propellant. Finally, using Equation 2.1.2, the estimated thrust value was found. In Equation 2.1.2, the first term on the right-hand side of the equation is known as the momentum thrust and the estimated value for this is about

5.4-lbf. The second term on the right-hand side of the equation is called the pressure thrust, and the estimated value for this is -3.5-lbf. A negative pressure thrust value means that the nozzle is over-expanded, and the static exit pressure of the engine is lower than the ambient pressure. This analytical estimation provides a value for thrust at around 1.8-lbf.

5.2 Preliminary Test Results

After the test stand had been designed and constructed, preliminary tests were conducted to find an optimal range of nozzle throat areas for an inlet pressure of 200-psi and a mass flow rate of 0.027-lb/s of NOS and a set burn time of 4-seconds. The nozzle sizes used for the preliminary tests include #13, #16, #19, and #25. These numbers indicate the diameter of the nozzle at the throat in 64ths of an inch. Figure 34 shows thrust curve profiles against burn time for each nozzle size. As a note for each thrust versus time graph in this study, all thrust curves will be lined up based on the beginning of the thrust descent after the solenoid has closed.

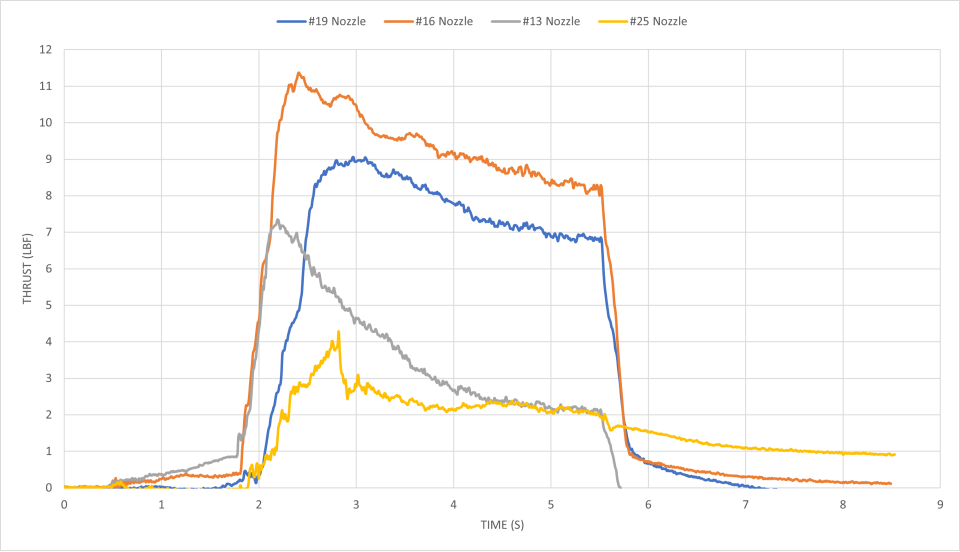

Figure 34: Hybrid Rocket Engine Performance for Various Nozzle Sizes

Each engine begins the test with the opening of the solenoid valve at around the 0.75-second mark and the rise in thrust due to ignition at the 1.75-second mark. After ignition

each engine configuration reached its peak thrust within 1-second and was then followed by a regressive thrust curve. This is typical of a Bates grain geometry. Table 6 shows the peak thrust, average thrust, total impulse, and specific impulse for each engine configuration.

Engine Number	Nozzle Size (#/64-in)	Peak Thrust (lbf)	Average Thrust (lbf)	Total Impulse (lbf-s)	Specific Impulse (s)
1	13	7.34	3.40	13.84	113.33
2	16	11.38	8.73	34.56	265.51
3	19	9.06	6.88	26.28	221.94
4	25	4.29	1.10	4.49	149.66

Table 6: Performance Parameters for Varying Nozzle Sizes

These test results show the optimal range of nozzle sizes for a feed pressure of 200-psi and an oxidizer mass flow rate of 0.027-lbm/s to be between a #16 and a #19 nozzle. These two nozzle sizes are then used to evaluate the test stand and statistical confidence levels of the thrust produced by the engine.

During the preliminary tests, a 3D printed solenoid support and orifice plate support were included to have the oxidizer feed system vertically in line with the engine casing. These supports were also bolted to the test stand table and could have had an impact on the thrust values recorded during testing. For the rest of the testing, the bolts were removed from the supports, but the supports were left in place. Additionally, manual quarter turn valves were added to the oxidizer feed system. One before the pressure regulator, and one after the solenoid but before the orifice plate. As mentioned previously, NOS has a self-pressurizing property, so at a temperature the pressure can also be known, Table 4. However, the temperature of NOS also goes up or down with the pressure. When the pressure regulator reduces the pressure of the NOS from 775-psi to 200-psi, the temperature of NOS drops to -20-°F. This temperature is outside the operating range of the solenoid valve, and because of this the solenoid was failing to completely close. With the addition of the manual quarter

turn valves, no undesired NOS will enter the engine and continue combustion.

5.3 #16 Nozzle Test Results

Figure 35 shows thrust curve profiles against burn time for the five tests completed with a #16 nozzle size, 50% cubic infill, and 200-psi feed pressure. Test 1 shows a neutral/regressive thrust curve; whereas test numbers 2 through 5 show neutral/progressive thrust curves. The variances in thrust curves could be due to minute differences in the 3D printed fuel grains and how well the NOS mixes with the PLA. Although the LabVIEW VI controls the opening/closing of the solenoid valve and ignition, the igniters used for this study have variance in how quickly they begin combustion between the PLA and NOS. This can be seen in the difference in rise time between all tests.

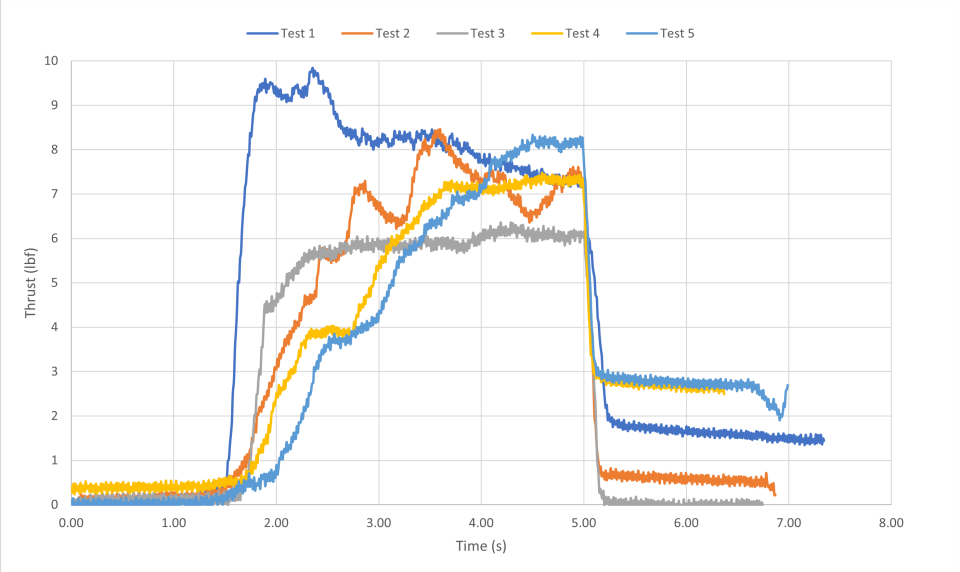

Figure 35: Tests with #16 Nozzle 50% Cubic Infill at 200-psi

Table 7 shows the performance parameters from each test with a #16 nozzle, as well as the average values and the percent standard deviation. Although burn time could be included in this table, as it is a typical performance parameter of other rocket types, it is not because the burn time is specifically controlled by the LabVIEW VI inputs.

As can be seen in the table the largest standard deviated parameter is the total impulse.

Performance Parameter	Test 1	Test 2	Test 3	Test 4	Test 5	Average	% Standard Deviation
Peak Thrust (lbf)	9.84	8.47	6.36	7.48	8.34	8.09	16%
Average Thrust (lbf)	7.91	6.06	5.50	5.41	5.37	6.05	18%
Total Impulse (lbf-s)	28.87	21.09	18.94	18.83	18.69	21.28	20%
Specific Impulse (s)	252.63	197.52	178.05	180.05	179.12	197.47	15%

Table 7: Performance Parameter Results with #16 Nozzle

All standard deviations are driven higher due to the high variance of Test 1, which had an unexpected increase in overall performance. Between the lowest and highest performing engine tests peak thrust varied by about 3.50-lbf, average thrust varied by 2.54-lbf, total impulse varied by 10.78-lbf-s, and the specific impulse varied by 74.58-s.

5.4 #19 Nozzle Test Results

Hybrid rocket engine test results completed with the #19 nozzle, 50% cubic infill geometry, and a feed pressure of 200-psi can be seen in Figure 36. The large variance in rise time seen with the #16 nozzle was not seen in the #19 nozzle tests; however, these tests reached lower peak and average thrust values. Which ultimately led to lower total and specific impulse values. The #19 tests were more consistent in their thrust profiles and thrust values. One note to make on the thrust curves for both the #16 and #19 nozzles is that the curves do not come back to zero at the end of the test. This is because the NOS freezes the spring inside the solenoid and does not allow it to close fully, allowing a portion of NOS to continue to flow to the casing continuing undesired combustion. Although it is not a significant amount of NOS it is obvious that there is some thrust produced from this latent combustion. The average thrust, total impulse, and specific impulse depend on the engine's burn time which is affected by this latent thrust because it does not allow the thrust curve to reach the 10% of peak thrust on descent. To adjust for this, the ending point for the burn time will

be considered the last point on the descending part of the thrust curve. This will slightly shorten the burn time, but not enough to significantly affect any performance parameters.

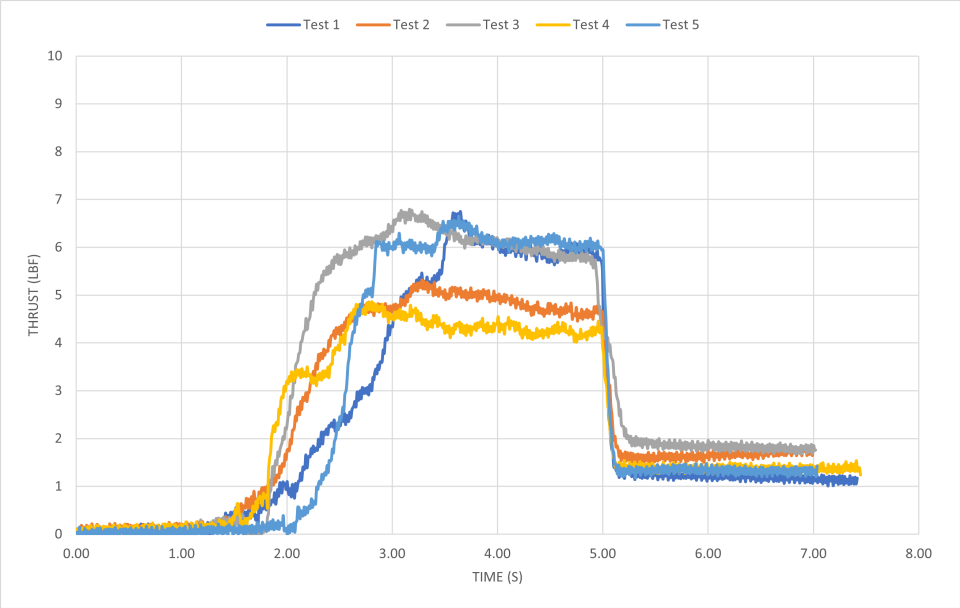

Figure 36: Tests with #19 Nozzle 50% Cubic Infill at 200-psi

Table 8 shows the performance parameters for each test with a #19 nozzle, as well as the average values and percent of standard deviation from the average. Between the lowest and highest performing engine tests peak thrust varied by about 1.94-lbf, average thrust varied by 1.46-lbf, total impulse varied by 5.16-lbf-s, and the specific impulse varied by 36.54-s.

Performance Parameter	Test 1	Test 2	Test 3	Test 4	Test 5	Average	% Standard Deviation
Peak Thrust (lbf)	6.74	5.32	6.80	4.86	6.65	6.07	15.1%
Average Thrust (lbf)	4.27	4.08	5.35	3.89	5.16	4.55	14.6%
Total Impulse (lbf-s)	14.53	14.40	18.68	13.52	15.61	15.35	13.1%
Specific Impulse (s)	141.74	127.59	164.13	128.03	154.22	143.14	11.2%

Table 8: Performance Parameter Results with #19 Nozzle

As can be seen in the table the performance of the #19 nozzle tests are more consistent

than that of the #16 nozzle tests. However, the #19 nozzle tests consistently provided lower average performance than the #16 nozzle tests. Lower performance by the #19 nozzle was seen in the preliminary testing, this trend continued throughout testing for this study.

5.5 Performance Parameter Results and Analysis

Table 9 displays all performance parameter results over the various nozzle sizes. The chart immediately serves as an overview of all tests and how they performed.

Hybrid Rocket Engine Mass Flow Rate Variation				
Test	Peak Thrust (lbf)	Average Thrust (lbf)	Total Impulse (lbf-s)	Specific Impulse (s)
16.2a	9.84	7.91	28.87	252.63
16.2b	8.47	6.06	21.09	197.52
16.2c	6.36	5.50	18.94	178.02
16.2d	7.48	5.41	18.83	180.05
16.2e	8.34	5.37	18.69	179.12
19.2a	6.74	4.27	14.53	141.74
19.2b	5.32	4.08	14.40	127.59
19.2c	6.80	5.35	18.68	164.13
19.2d	4.86	3.89	13.52	128.03
19.2e	6.65	5.16	15.61	154.22

Table 9: Performance Parameters for Various Nozzle Sizes

Also, hypothesis testing through a series of Student T-tests was conducted at a 90% confidence level for all discussed performance parameters. Using the Students T-test table [51] found in Appendix 2 at an α of 0.1 and 8 degrees of freedom, the T-value being used for this study is 1.397. If the test statistic calculated from the hybrid rocket tests is larger than the value from the table this means the test stand is statistically able to detect differences

in the performance between the two nozzle sizes. If the calculated test statistic, on the other hand, is smaller than the T-value from the table, this means the test stand was not able to differentiate between the two nozzle sizes. A P-value was then found from the test statistic to show the significance of the difference in means of each performance parameter. If the P-value is lower than 0.1 this means the test stand was able to significantly differentiate between the two test cases. Additionally, confidence intervals were created at a 90% confidence level for each performance parameter (peak thrust, average thrust, total impulse, and specific impulse). Confidence intervals show a range in which the true difference between two samples means, and help to identify the uncertainty in the calculated t distribution test statistic.

5.5.1 Peak Thrust

Average values of peak thrust achieved for each nozzle size can be observed in Table 10 along with their respective percent standard deviations and error bars. The error bar values in the table are used to provide the range for which the standard deviation will fall for the peak thrust.

Test	Average Peak Thrust (lbf)	Peak Thrust (% Std Dev)	Error Bar (+/- lbf)
16.2	8.10	15.90%	0.64
19.2	6.07	15.09%	0.46

Table 10: Peak Thrust Performance for Variations in Nozzle Sizes

The table shows the #19 nozzle has a slightly lower percent standard deviation than the #16 nozzle meaning it is more consistent. This can also be seen in the error bar values, which are also dependent on the peak thrust. Between the lowest point of the error bar for the #16 nozzle and the highest point of the error bar for the #19 nozzle is almost a pound of thrust. This provided some level of confidence, but a statistical analysis was still necessary. After completing the error bar analysis, a T-test was completed for peak thrust. Table 11

shows the results from this T-test analysis.

Comparison	Variance #16	Variance #19	Difference of Averages	Calculated T-value
16 - 19	1.65	0.84	2.02	2.86

Table 11: Peak Thrust Equal Variance Result for #16 vs. #19 Nozzle Sizes

The t test results dictate the test stand can accurately differentiate between #16 and #19 nozzle sizes at a 90% confidence level. Showing the test stand works as designed. The resulting P-value from the calculated test statistic for peak thrust was 0.01, showing the peak thrust values from the #16 and #19 nozzles to be significantly different. Also, a confidence interval was found for peak thrust. With 90% confidence the difference in mean peak thrust between the #16 and #19 nozzle sizes is between 1.04-lbf and 3.00-lbf. This confidence interval was found using a critical t value of 1.397, a standard error of 0.707, an error margin of 0.99, and the difference of means for peak thrust.

5.5.2 Average Thrust

Average values of average thrust reached for each nozzle size can be seen in Table 12 along with their respective percent standard deviation and error bars.

Test	Average Thrust (lbf)	Average Thrust (% Std Dev)	Error Bar (+/- lbf)
16.2	6.05	18%	0.54
19.2	4.55	14.5%	0.33

Table 12: Average Thrust Performance for Variations in Nozzle Sizes

As seen in Table 12, between the lower bound of the #16 nozzle error bar and the upper bound of the #19 nozzle error bar there is a difference of 0.63 pounds. This value is less

than that for peak thrust, but there is clearly a difference in average thrust values. Also, from Table 12, the #19 nozzle has a lower percent standard deviation than the #16 nozzle provided, meaning the #19 shows more consistency between tests. Once again, a T-test was conducted on the average thrust values. Table 13 shows the results from the T-test analysis with eight degrees of freedom at a 90% confidence level.

Comparison	Variance #16	Variance #19	Difference of Averages	Calculated T-value
16 - 19	1.16	0.43	1.50	2.65

Table 13: Average Thrust Equal Variance Result for #16 vs. #19 Nozzle Sizes

The results from Table 13 prove there is a 90% statistical confidence that the average values for the average thrust are different between the two nozzle sizes. This, along with the T-test from the peak thrust helps to show the validity of the test stand design. The resulting P-value from the calculated test statistic for average thrust was 0.014, showing the average thrust values from the #16 and #19 nozzles to be significantly different. Also, a confidence interval was found for average thrust. With 90% confidence the difference in mean average thrust between the #16 and #19 nozzle sizes is between 0.71-lbf and 2.29-lbf. This confidence interval was found using a critical t value of 1.397, a standard error of 0.57, an error margin of 0.79, and the difference of means for average thrust.

5.5.3 Total Impulse

Table 14 shows average values of total impulse reached for each nozzle size along with their respective percent standard deviation and error bars.

Table 14 shows the difference between the low end of the #16 nozzle and the upper end of the #19 nozzle to be 2.75-lbf-s. This is a higher value than both the peak and average thrust value error bar differences, but it is because the burn time is incorporated into the total impulse calculation and magnifies the values. Like the peak and average thrust values,

Test	Average Total Impulse (lbf-s)	Average Total Impulse (% Std Dev)	Error Bar (+/- lbf*s)
16.2	21.28	20%	2.18
19.2	15.35	13%	1.00

Table 14: Total Impulse Performance for Variations in Nozzle Sizes

a T-test was completed for total impulse values. Table 15 shows the results from the T-test analysis with a 90% confidence level and eight degrees of freedom. The difference between this T-test and the two previous T-tests is that the variances were not assumed to be equal. Variances can be assumed to be equal if the ratio between variances is less than 4. For all previous performance parameters, this was the case, but for total impulse they are not. The only difference between T-tests with equal and unequal variances is a slight variation in the calculation of the test statistic.

Comparison	Variance #16	Variance #19	Difference of Averages	Calculated T-value
16 - 19	18.97	4.02	5.93	1.53

Table 15: Total Impulse Equal Variance Result for #16 vs. #19 Nozzle Sizes

Despite the variances not being equal for the calculation of the test statistic, the resulting value is still greater than the value from the table. This shows that the average total impulses between the two samples are different at a 90% confidence level, once again showing the test stand works as designed. The resulting P-value from the calculated test statistic for total impulse was 0.012, showing the total impulse values from the #16 and #19 nozzles to be significantly different. Also, a confidence interval was found for total impulse. With 90% confidence the difference in mean total impulse between the #16 and #19 nozzle sizes is between 2.94-lbf-s and 8.93-lbf-s. This confidence interval was found using a critical t value of 1.397, a standard error of 2.14, an error margin of 2.99, and the difference of means for

total impulse.

5.5.4 Specific Impulse

Average values of specific impulse achieved for each nozzle size can be observed in Table 16 along with their respective percent standard deviation and error bars.

Test	Average Specific Impulse (lbf-s)	Average Specific Impulse (% Std Dev)	Error Bar (+/- s)
16.2	197.47	16%	15.93
19.2	143.14	11.25%	8.05

Table 16: Specific Impulse Performance for Variations in Nozzle Sizes

Table 16 shows the lowest point of the #16 nozzle error bar and the highest point of the #19 nozzle error bar to be 46.44-s apart from each other. This value is even higher than that of the total impulse, but because the average thrust is divided by the weight flow rate of the propellant any slight deviation in average thrust will have a large impact on the specific impulse. The weight flow rate of propellant is less than one which is why the values are so large. The final T-test done for the study can be found in Table 17.

Comparison	Variance #16	Variance #19	Difference of Averages	Calculated T-value
16 - 19	1015.27	258.91	54.32	3.40

Table 17: Specific Impulse Equal Variance Result for #16 vs. #19 Nozzle Sizes

Table 17 shows the averages of specific impulse for the testing completed for this study are different at a 90% confidence level. The resulting P-value from the calculated test statistic for specific impulse was 0.004, showing the specific impulse values from the #16 and #19 nozzles to be significantly different. Additionally, a final confidence interval was created for

specific impulse. With 90% confidence the difference in mean specific impulse between the #16 and #19 nozzle sizes is between 32.03-s and 76.62-s. This confidence interval was found using a critical t value of 1.397, a standard error of 15.96, an error margin of 22.30, and the difference of means for peak thrust.

5.5.5 Performance Parameter Overview

Table 18 below summarizes differences between the #16 and #19 statistical test results including P-values and confidence intervals all at a 90% confidence level.

Performance Parameter	#16 Nozzle Mean	#19 Nozzle Mean	P-Value	Confidence Interval
Peak Thrust (lbf)	8.10	6.07	0.01	(1.04, 3.00)
Average Thrust (lbf)	6.05	4.55	0.014	(0.71, 2.92)
Total Impulse (lbf-s)	21.28	15.35	0.012	(2.94, 8.93)
Specific Impulse (s)	197.47	143.14	0.004	(32.03, 76.62)

Table 18: Performance Parameter Statistical Overview

Table 18 shows the test stand was statistically able to differentiate between the #16 nozzle testing configuration and the #19 nozzle testing configuration at each performance parameter focused on throughout this study. The testing results from this study show the test stand is capable of differentiating between various configurations and test setups.

5.5.6 Ensemble Thrust Profile Analysis

To observe the consistency of thrust profiles achieved by each nozzle size, an ensemble averages were created for each testing configuration. Table 19 below displays average thrust profile percent deviations over the course of each engine's entire burn. Additionally, a measure of how well each motor consistently met its ensemble average deviation is captured.

This is done through taking the standard deviation of all the percent thrust deviations that occurred at each point represented in each ensemble thrust profile.

Test	Ensemble Thrust Profile (Average % Std Dev)	Deviation of Ensemble % Std Dev (%)
16	43%	39%
19	37%	36%

Table 19: Ensemble Thrust Profile Average Deviation and Deviation Consistency for Variations in Nozzle Sizes

From the table above, overall thrust profiles of tests with the #19 nozzle deviated less than tests with the #16 nozzle. In Figure 37 ensemble thrust profiles for #16 and #19 nozzle sizes can be viewed, with their error bars representing thrust standard deviation at each point throughout their burns.

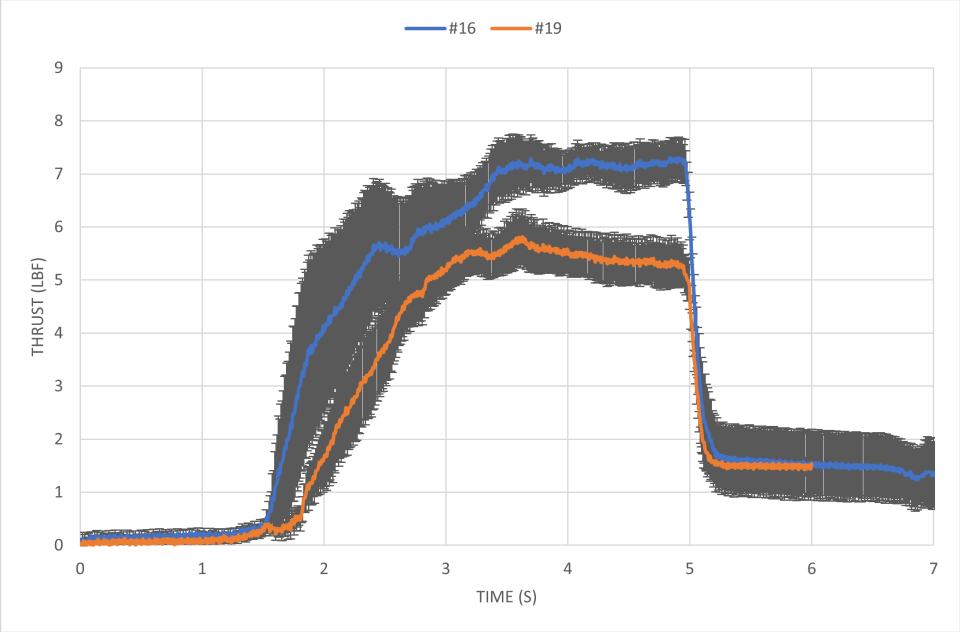

Figure 37: Ensemble Thrust Profiles for #16 and #19 Nozzle Configurations

While the average percent standard deviation for #16 and #19 nozzles are equal to 43% and 37%, respectively, the #19 nozzle tests were able to maintain its 37% deviation much

more consistently than its #16 nozzle counterpart. This is observed in that #19 nozzles percent standard deviation of all the deviations making up the ensemble average sits at 36% while the #16 nozzles come in at 39%. This trend appears to be consistent with Figure 37 as it is apparent that the amount of error around the #16 nozzle ensemble curve grows on the initial rise, while the #19 nozzle remains constant throughout. As can be seen in the above figure the rise in the thrust curves seem to be similar, with the #16 nozzle having a slightly steeper slope. However, after the initial rise the thrust curves show a significant difference in shape towards the end of the burn.

5.5.7 Rise Ensemble Profile

Along with an overall ensemble analysis, as seen above, additional ensemble analyses were completed for two stages throughout the tests. These two stages are characterized as rise ensemble and steady burn ensemble.

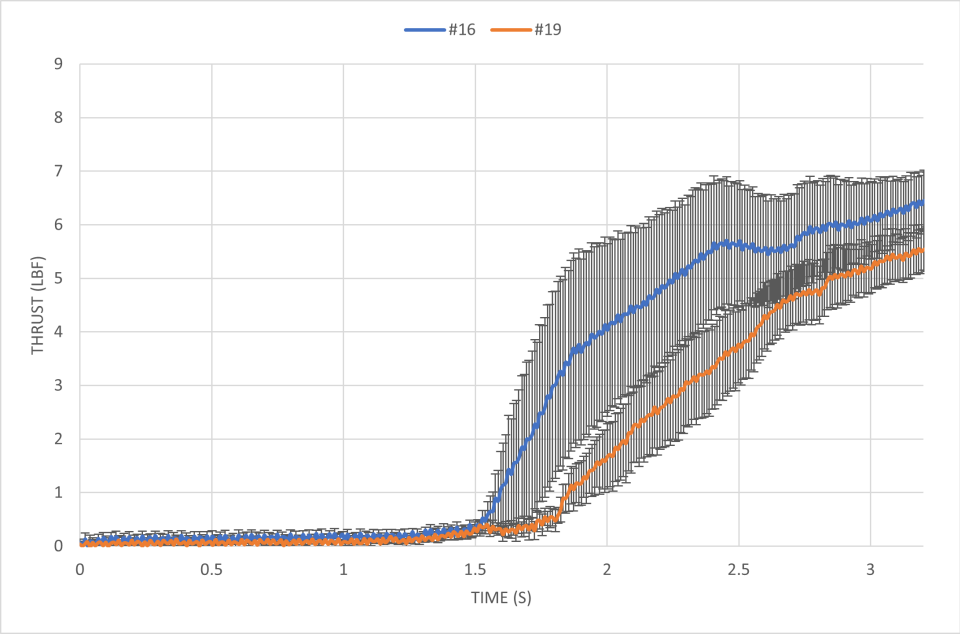

Figure 38: Ensemble Thrust Profiles for #16 and #19 Nozzle Configurations Time 0-3.2 Seconds

The ensemble profiles do not change from Figure 37; however, the rise ensemble profile

section focuses on the first 3 seconds of the ensemble profile and the steady ensemble profile section focuses on the last 2 seconds of the overall ensemble profile. The purpose of splitting the overall thrust profile into two sections is because of the igniter variance and the increased deviation from the average curve during the first three seconds of the burn profile. During the first three seconds of all tests, there are no major differences in thrust curves between the #16 and #19 nozzle testing configurations. These thrust profiles can be seen in Figure 38. The error bars of the two curves cross between 2.5-3.2 seconds and show that at this point in the test the leading contributor to thrust is due to the igniter, and the reason the two curves overlap is because of the variance in igniter performance.

5.5.8 Steady Ensemble Profile

Once combustion begins, around the 3.2-second mark, the curves of the two different nozzle sizes begin to separate and stay apart from each other for the duration of the test. At this point it is clear the effect the nozzle has on the performance of the engine.

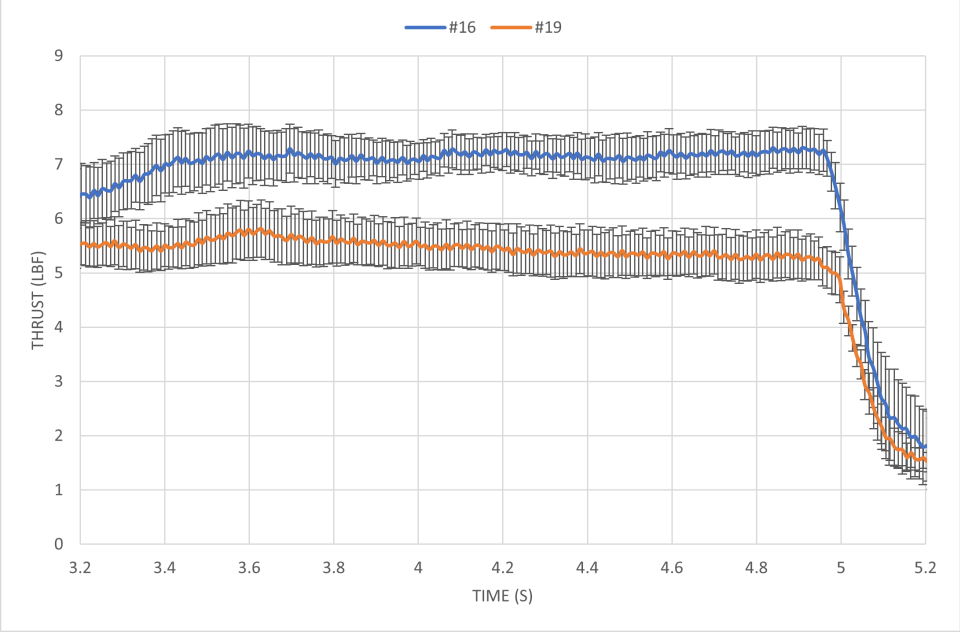

Figure 39: Ensemble Thrust Profiles for #16 and #19 Nozzle Configurations Time 3.2-5.2 Seconds

The smaller #16 nozzle begins to increase the chamber pressure to a point that increases the thrust output, whereas the #19 nozzle increases chamber pressure, but not enough to increase the thrust as much as the #16 nozzle configuration does. The separation of the two thrust curves can be seen in Figure 39

5.6 Mass Flow Rate Test Results

Although the testing for this study mainly focused on the changing of mass flow rates by varying nozzle areas, additional tests were conducted at various feed pressures. One test was completed at a feed pressure of 300-psi and another at 400-psi. These tests were conducted with a #16 nozzle size because of the increased performance with this nozzle size as compared to others. The data from these tests were then compared with the average thrust curve produced by the #16 nozzle at 200-psi. Figure 40 shows these three curves.

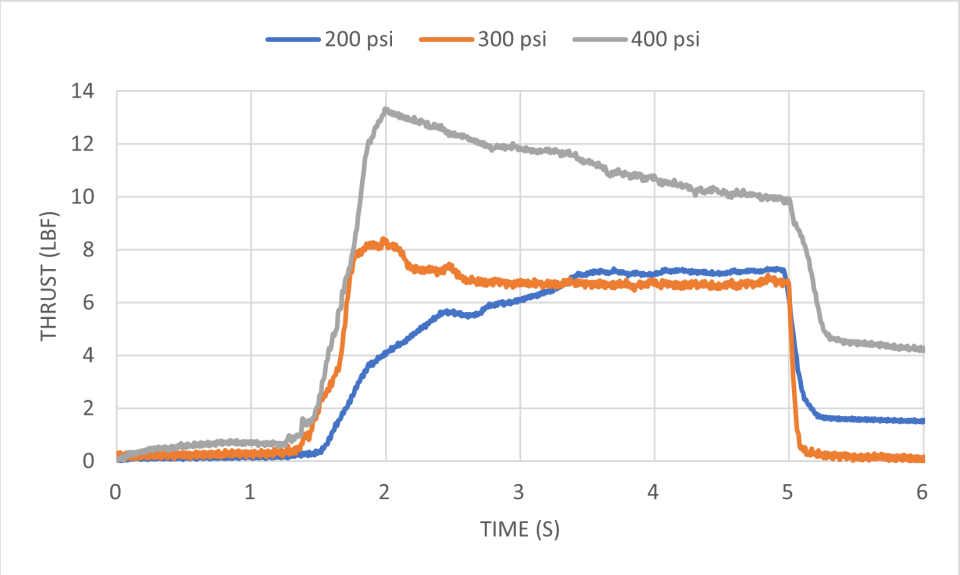

Figure 40: Thrust Curves with Varying Feed Pressures

As can be seen in the figure, there is not a large difference in thrust curve profile between the 200-psi average and the 300-psi test near the end of the curve. The main difference between the average 200-psi and the 300-psi curves is on the initial rise. As documented before, this could be due to a variance in igniter performance. Once the 300-psi thrust curve

levels out after the initial rise it becomes linear. However, there seems to be a significant difference between the 400-psi test and all other tests. The initial rise of the 300-psi and 400-psi tests lie on top of each other, but the curve continues to rise to its peak at around 13.3-lbf. This was the best performing test in the whole study. This is also indicated by the performance parameter values found in Table 20.

Pressure (psi)	Peak Thrust (lbf)	Average Thrust (lbf)	Total Impulse (lbf-s)	Specific Impulse (s)
200	8.10	6.05	21.28	197.47
300	8.42	6.49	23.87	148.68
400	13.34	10.29	40.28	178.86

Table 20: Performance Parameters for Varying Feed Pressure

While no statistical analysis was completed for the varying pressure tests because of the small sample size, it does seem as though there is a significant increase in peak thrust, average thrust, and total impulse. There is not necessarily an increase in specific impulse despite the increase in average thrust, there is also an increase in exhausted mass flow which brings down the specific impulse value.

5.7 Test Stand Results

The main objective of this study is to design and evaluate a hybrid rocket test stand. Although the results of all tests have been discussed, it is important to note how the stand performed and how well it held up throughout the rigorous testing completed. The structural design of the stand held up as designed; each fitting, nut, bolt, and screw was consistently checked between tests. During these routine checks, no component was ever loose or out of place. The test stand proved to be able to hold the loads provided by the engine and will be able to handle much larger tests in future studies.

CHAPTER VI

CONCLUSIONS

6.1 Research Objectives and Outcomes

6.1.1 Evaluation of Test Stand Design

The primary goal of this study was to design, build, and evaluate a hybrid rocket test stand. The constructed test stand works as designed and held up cleanly throughout all testing. The fittings, nuts, bolts, and rods showed no signs of loosening or deteriorating throughout testing. Although, periodically checking the fitment and tightness of all components would help to lengthen the lifespan of the stand. The linear bearings and aluminum plate construction was strong during testing and did not restrict the thrust load from being delivered to the load cell. The oxidizer feed system also held up well; however, two notes should be made. Firstly, a different solenoid should be used that can handle the low temperatures after the pressure of the NOS has been regulated. Second note, is the pressure regulator needs to be lubricated regularly to ensure proper regulation of the NOS. Other than this the feed system worked smoothly. The LabVIEW VI allowed for consistent timing of the solenoid opening and closing as well as ignition. The main variation in the test stand itself would be the igniter, this is not necessarily a problem with the LabVIEW program, but instead the inconsistencies of the igniters and how well the leads are contacting the pyrogen propellant.

As discussed previously the evaluation of the test stand involved physical tests as well as a statistical analysis to determine if the stand could differentiate between various engine configurations. The test stand was very good at differentiating average values for peak

thrust, average thrust, total impulse and specific impulse. All statistical analysis was done at a 90% confidence level.

6.1.2 Evaluation of the Effectiveness of the #16 Nozzle

When looking at the test results, the effect the #16 nozzle had on the hybrid rocket engine performance was very positive. It increased all performance values when compared to other nozzle sizes. Test 1 showed some inconsistency on the burn profile, but still reached a higher peak thrust value than any other test at a feed pressure of 200-psi. All other tests were consistent in their thrust curves and peak thrust values. More testing should be done with this configuration to continue to increase confidence that this nozzle size provides the best performance in the range of nozzle sizes tested throughout this study.

6.1.3 Evaluation of the Effectiveness of the #19 Nozzle

The #19 nozzle like the #16 nozzle was within the optimal range of nozzle sizes determined in the preliminary testing. Although, the #19 nozzle provided lower performance values across the board, the tests were more consistent at this nozzle size shown by a decreased values in the percent standard deviations of the performance parameters. Additional testing would be helpful to increase confidence that the #19 nozzle provides these consistent values.

6.1.4 Evaluation of the Effectiveness of Changing Feed Pressure

While no statistical analysis was completed on the tests where feed pressures were varied, some conclusions may still be made. From Figure 40 it obvious that the 400-psi test outperformed its 200-psi and 300-psi counterparts. Although the 400-psi test provided higher performance in peak thrust, average thrust, and total thrust; the specific impulse was lower than that of the average 200-psi data. Also, the 400-psi test increased the mass flow rate of the PLA. Even though this is the case, eye-witnessing testing showed non-combusted PLA being ejected from the nozzle at a feed pressure of 400-psi which would decrease the actual

amount of PLA being burnt during the test. Future testing should include a larger sample size of various feed pressures in order to ascertain the most efficient feed pressure and regression rate of the PLA, as well as a way to gauge the mass of PLA being burnt versus the mass of solid PLA being ejected from the nozzle.

6.2 Final Remarks and Recommendations

This study proved the effectiveness of the test stand for a specific combination of fuel and oxidizer at a limited range of mass flow rates. As a result, small sample sizes were used. A narrowed approach to the issue of hybrid rocket performance would allow for increased testing to occur within selected configurations, allowing for an increased level of confidence in results. Also, the only data collection performed in this study were values of thrust produced against burn duration. Future studies, that evaluate the design of the test stand, should include incorporating recording of chamber pressure to validate thrust profiles and analyze pressure variations that would have influence on hybrid rocket engine combustion stability. Other components that could be included in the test stand design are load cells directly under the combustion chamber to determine the time dependent mass flux of the fuel grain, and incorporating a thermocouple either in the exhaust stream or in the combustion chamber to have a better understanding of the combustion characteristics of the engine. Other studies could focus specifically on the design of the solid fuel grain including varying infill percentage, infill geometry, port geometry, and fuel grain composition. Dealing with the hardware aspect of the test stand, studies focusing on pre, and post combustion chambers should be done in order to determine the performance effects of these components. Lastly, performance evaluations have only been completed at a singular combustion chamber diameter of 1.5-in (38-mm) and length of 7-in. Studies at the standard neighboring chamber sizes of 2.13-in (54-mm) and 3-in (76-mm), and standard chamber lengths associated with the chamber sizes should be had to assess the viability of the test stand design. This study allows for further hybrid rocket engine experimentation that can now expand to varying mass flow rates, fuels,

oxidizers, and engine sizes to be further evaluated on performance and consistency. In all future tests conducted on the test stand, testing lengths should be increased to see the affect of steady combustion on thrust as seen in the splitting of ensemble analyses. Depending on the application of the hybrid rocket engine, future development of the test stand could include varying the orientation of the test stand if the engine would be used in a vertical launch scenario.

REFERENCES

[1] Aerospace Notes. Hybrid rocket propulsion, Feb 2021.

[2] George P Sutton and Oscar Biblarz. *Rocket Propulsion Elements*. John Wiley & Sons, 2016.

[3] L.T. DeLuca, L. Galfetti, F. Maggi, G. Colombo, L. Merotto, M. Boiocchi, C. Paravan, A. Reina, P. Tadini, and L. Fanton. Characterization of htpb-based solid fuel formulations: Performance, mechanical properties, and pollution. *Acta Astronautica*, 92(2):150–162, 2013. 2nd IAA Symposium on Private Human Access to Space.

[4] Dario Pastrone. Approaches to low fuel regression rate in hybrid rocket engines. *International Journal of Aerospace Engineering*, 2012(1):75–86, 2012.

[5] E. WONG. *Solid rocket nozzle design summary*, chapter 1, pages 1–16. AIAA, 1968.

[6] S.S Heister, J.D Anderson, M.L Pourpoint, and G.R Cassady. *Rocket Propulsion*. John Wiley & Sons, 2012.

[7] Wikipedia. Rocket engine nozzle — Wikipedia, the free encyclopedia, 2022.

[8] Jack D. Mattingly and Keith M. Boyer. *Elements of propulsion: Gas turbines and rockets*. AIAA, 2016.

[9] N.A. Davydenko, R.G. Gollender, A.M. Gubertov, V.V. Mironov, and N.N. Volkov. Hybrid rocket engines: The benefits and prospects. *Aerospace Science and Technology*, 11(1):55–60, 2007. Propellant combustion phenomena.

[10] D. P. MISHRA. *Fundamentals of Rocket Propulsion*. CRC PRESS, 2020.

[11] M. C. Ventura and S. D. Heister. Hydrogen peroxide as an alternate oxidizer for a hybrid rocket booster. *Journal of Propulsion and Power*, 11(3):562–565, 1995.

[12] John Campbell, Frank Macklin, and Zachary Thicksten. *Handling Considerations of Nitrous Oxide in Hybrid Rocket Motor Testing*, chapter 1, pages 1–7. AIAA, 2008.

[13] G. Story. *Large-Scale Hybrid Motor Testing*, chapter 13, pages 513–552. AIAA, 2012.

[14] M. Kobald, U. Fischer, K. Tomilin, A. Petrarolo, and C. Schmierer. Hybrid experimental rocket stuttgart: A low-cost technology demonstrator. *Journal of Spacecraft and Rockets*, 55(2):484–500, 2018.

[15] Daisuke Nakata, Kazuki Yasuda, Shuhei Horio, and Kazuyuki Higashino. *A Fundamental Study on the Hybrid Rocket Clustering for the Rocket Sled Propulsion System*, chapter 1, pages 1–11. AIAA, 2016.

[16] Yen-Sen Chen and Bill Wu. *Development of a Small Launch Vehicle with Hybrid Rocket Propulsion*, chapter 1, pages 1–9. AIAA, 2018.

[17] Hamed Gamal, Adam Matusiewicz, Robert Magiera, David Hubert, and Lukasz Karolewski. *Design, Analysis and Testing of a Hybrid Rocket Engine with a Multi-Port Nozzle*, chapter 1, pages 1–15. AIAA, 2018.

[18] Cagri Oztan and Victoria Coverstone. Utilization of additive manufacturing in hybrid rocket technology: A review. *Acta Astronautica*, 180:130–140, 2021.

[19] McFarland and Antunes. Small-scale static fire tests of 3d printing hybrid rocket fuel grains produced from different materials. *Aerospace*, 6(7):81, Jul 2019.

[20] Stephen A. Whitmore, Zachary W. Peterson, and Shannon D. Eilers. Comparing hydroxyl terminated polybutadiene and acrylonitrile butadiene styrene as hybrid rocket fuels. *Journal of Propulsion and Power*, 29(3):582–592, 2013.

[21] Byeonguk Ahn, Jeongmoo Huh, Vikas Khandu Bhosale, and Sejin Kwon. Three-dimensionally printed polylactic acid as solid fuel for hydrogen peroxide hybrid rockets. *Journal of Propulsion and Power*, 37(1):171–175, 2021.

[22] Yi-Chi Chien, Chenju Liang, Shou-Heng Liu, and Shu-Hua Yang. Combustion kinetics and emission characteristics of polycyclic aromatic hydrocarbons from polylactic acid combustion. *Journal of the Air & Waste Management Association*, 60(7):849–855, 2010.

[23] Wikipedia. Polylactic acid, Jan 2023.

[24] Hongmei Chen, Fengyi Chen, Hui Chen, Hongsheng Liu, Ling Chen, and Long Yu. Thermal degradation and combustion properties of most popular synthetic biodegradable polymers. *Waste Management & Research*, 0(0):1–11, 2022. PMID: 36250214.

[25] D. Velasco. Evaluation of granular distribution and propellant grain length on tri-modal ammonium perchlorate solid rocket motors. Master's thesis, Oklahoma State University, 05 2022.

[26] Stephen A. Whitmore, Sean D. Walker, Daniel P. Merkley, and Mansour Sobbi. High regression rate hybrid rocket fuel grains with helical port structures. *Journal of Propulsion and Power*, 31(6):1727–1738, 2015.

[27] James C. Thomas, Eric L. Petersen, John D. Desain, and Brian Brady. *Hybrid Rocket Enhancement by Micro- and Nano-Scale Additives in HTPB Fuel Grains*, chapter 1. AIAA, 2015.

[28] Wikipedia. Hybrid rocket fuel regression, May 2022.

[29] Apogee Rockets. Apogee components - first fire starter for high power motors.

[30] Adam Okninski, Wioleta Kopacz, Damian Kaniewski, and Kamil Sobczak. Hybrid rocket propulsion technology for space transportation revisited - propellant solutions and challenges. *FirePhysChem*, 1(4):260–271, 2021. Progress in Hybrid Rocket Propulsion.

[31] W6Store. Nos bottles, 2012.

[32] Nitrous Outlet. Wrap around n2o heater element for mother bottle.

[33] Dalko H. Jeri. Design and construction of a hybrid rocket propulsion system. Technical report, University of Colorado at Denver, 2020.

[34] Lucas Carolo. What is fdm 3d printing? – simply explained, Nov 2022.

[35] Matt Tyson. Advanced guide to printing pla filament, May 2018.

[36] James Thomas, Jacob Stahl, Gordon Morrow, and Eric Petersen. Design of a lab-scale hybrid rocket test stand. In *Propulsion Energy Forum*, 07 2016.

[37] Mohammed Bouziane, Artur Bertoldi, Praskovia Milova, P. Hendrick, and Michel Lefebvre. Development and testing of a lab-scale test-bench for hybrid rocket engines. In *Space Ops Conference*, 05 2018.

[38] Matt H. Summers. Small-scale hybrid rocket test stand & characterization of swirl injectors. Master's thesis, Arizona State University, 04 2013.

[39] Jeffrey Kozak. Overview of the hybrid rocket design.

[40] Lucas Utley, Garrett Foster, and Kurt Rouser. Design and evaluation of a portable, flexible-use rocket thrust stand.

[41] II Freeman, Chuck W. *Solid Rocket Motor Static Fire Test Stand Optimization: Load Cell Effects and Other Uncertainties*. PhD thesis, University of Alabama in Huntsville, 2018.

[42] Jeff Smith. Ask away: Optimizing your nitrous system with proper bottle pressure, Jul 2022.

[43] Wikipedia. Nitrous oxide, Feb 2023.

[44] Ronald W. Humble, Gary N. Henry, and Wiley J. Larson. *Space Propulsion Analysis and design*. McGraw-Hill, 2007.

[45] Phillip M. Gerhart, Andrew L. Gerhart, and John I. Hochstein. *Munson, Young, and Okiishi's Fundamentals of Fluid Mechanics*. Wiley, 8 edition, 2013.

[46] Creality. Ender 5 printer guide book, 2019.

[47] Benjamin Goldschmidt. Cura guide to the best infill patterns, Nov 2022.

[48] Nitrous Outlet. Nitrous outlet pump station & scale.

[49] High power rocket safety code - national association of rocketry, Sep 2022.

[50] Chris Snyder. Cearun rev3c, April 2023.

[51] Students t table, Apr 2021.

APPENDICES

Appendix 1

Oxidizer Feed Valve Analysis

Tank pressure & temperature, as well as MFP for choked inlet valve:

$P_t := 200psi$ $T_t := (72 + 460)R = 532 \cdot R$ $MFP_{in} := 0.63866 \frac{lbm \cdot \sqrt{R}}{lbf \cdot s}$ (Assuming $\gamma = 1.3$)

Maybe... if 5/64 is diameter (probably not):

$D_t := \frac{5}{64} in = 1.984 \cdot mm$ $A_{eff} := \pi \cdot \left(\frac{D_t}{2}\right)^2 = 4.794 \times 10^{-3} \cdot in^2$ $m\_dot_{ox1} := \frac{MFP_{in} \cdot A_{eff} \cdot P_t}{\sqrt{T_t}} = 0.027 \cdot \frac{lbm}{s}$

Nozzle Flow Analysis:

Measured mass flow ratio of oxidizer to fuel based on measured mass flow rate of fuel:

$m\_dot_{fuel} := 0.0033 \frac{lbm}{s}$ $f_{o\_f} := \frac{m\_dot_{ox1}}{m\_dot_{fuel}} = 8.045$ $m\_dot_{total} := m\_dot_{ox1} + m\_dot_{fuel} = 0.03 \cdot \frac{lbm}{s}$

(verify fuel mass flow rate experimentally by measuring burn time and mass before & after test)

Assume MFP for choked nozzle: $MFP_{th} := 0.63341 \frac{lbm \cdot \sqrt{R}}{lbf \cdot s}$ (Assuming $\gamma = 1.27$)

Medium nozzle... Select nozzle throat diameter: $D_{th} := \frac{16}{64} in$ $A_{th} := \pi \cdot \left(\frac{D_t}{2}\right)^2 = 0.049 \cdot in^2$

Adjust chamber pressure (can be greater than tank pressure) and combustion temperature:

$P_c := 60psi = 4.137 \times 10^5 Pa$ $T_c := (3500 + 460)R = 3.96 \times 10^3 \cdot R$

$m\_dot_{th} := \frac{MFP_{th} \cdot A_{th} \cdot P_c}{\sqrt{T_c}} = 0.03 \cdot \frac{lbm}{s}$ (should closely match m_dot_{total} estimate above)

Analytical Thrust Estimation T=2960K and P=56psi:

Constants: $g_c := 32.2 \frac{lbm \cdot ft}{lbf \cdot s^2}$ $\gamma_{cea} := 1.2988$ $M_t := 1$ $c_{p1} := 1.2286 \frac{J}{gm \cdot K}$ $P_{amb} := 13.98psi$

Assumptions: $T_{throat} := 3960R$ $P_{throat} := 60psi$

Output from GasTabs: $M_e := 3.01$

Isentropic Temp Relation: $Tte\_T_e := 1 + \frac{\gamma_{cea} - 1}{2} \cdot M_e^2 = 2.354$

Figure 41: Analytical Estimation Page 1

Isentropic Pressure Relation: $Pte\_P_e := \left(1 + \frac{\gamma_{cea} - 1}{2} \cdot M_e^2\right)^{\frac{\gamma_{cea}}{\gamma_{cea} - 1}} = 41.286$

Static Temp at Exit: $T_e := \frac{T_{throat}}{Tte\_T_e} = 1.683 \times 10^3 \cdot R$ $R_{cea} := \frac{c_{p1} \cdot (\gamma_{cea} - 1)}{\gamma_{cea}} = 0.283 \frac{J}{gm \cdot K}$

Static Pressure at Exit: $P_e := \frac{P_{throat}}{Pte\_P_e} = 1.453 \cdot psi$

Exit Velocity: $V_e := M_e \cdot \sqrt{\gamma_{cea} \cdot R_{cea} \cdot T_e \cdot g_c} = 5.787 \times 10^3 \cdot \frac{ft}{s}$

#16 Nozzle d_e and A_e: $d_e := 0.6in$ $A_e := \frac{\pi \cdot d_e^2}{4} = 0.283 \cdot in^2$

Momentum Thrust: $F_{mom} := m\_dot_{total} \cdot V_e = 5.369 \cdot lbf$

Pressure Thrust: $F_{pressure} := (P_e - P_{amb}) \cdot A_e = -3.542 \cdot lbf$

Total Thrust: $F_{total} := F_{mom} + F_{pressure} = 1.827 \cdot lbf$

Figure 42: Analytical Estimation Page 2

Appendix 2

t Table

cum. prob	$t_{.50}$	$t_{.75}$	$t_{.80}$	$t_{.85}$	$t_{.90}$	$t_{.95}$	$t_{.975}$	$t_{.99}$	$t_{.995}$	$t_{.999}$	$t_{.9995}$
one-tail	0.50	0.25	0.20	0.15	0.10	0.05	0.025	0.01	0.005	0.001	0.0005
two-tails	1.00	0.50	0.40	0.30	0.20	0.10	0.05	0.02	0.01	0.002	0.001
df											
1	0.000	1.000	1.376	1.963	3.078	6.314	12.71	31.82	63.66	318.31	636.62
2	0.000	0.816	1.061	1.386	1.886	2.920	4.303	6.965	9.925	22.327	31.599
3	0.000	0.765	0.978	1.250	1.638	2.353	3.182	4.541	5.841	10.215	12.924
4	0.000	0.741	0.941	1.190	1.533	2.132	2.776	3.747	4.604	7.173	8.610
5	0.000	0.727	0.920	1.156	1.476	2.015	2.571	3.365	4.032	5.893	6.869
6	0.000	0.718	0.906	1.134	1.440	1.943	2.447	3.143	3.707	5.208	5.959
7	0.000	0.711	0.896	1.119	1.415	1.895	2.365	2.998	3.499	4.785	5.408
8	0.000	0.706	0.889	1.108	1.397	1.860	2.306	2.896	3.355	4.501	5.041
9	0.000	0.703	0.883	1.100	1.383	1.833	2.262	2.821	3.250	4.297	4.781
10	0.000	0.700	0.879	1.093	1.372	1.812	2.228	2.764	3.169	4.144	4.587
11	0.000	0.697	0.876	1.088	1.363	1.796	2.201	2.718	3.106	4.025	4.437
12	0.000	0.695	0.873	1.083	1.356	1.782	2.179	2.681	3.055	3.930	4.318
13	0.000	0.694	0.870	1.079	1.350	1.771	2.160	2.650	3.012	3.852	4.221
14	0.000	0.692	0.868	1.076	1.345	1.761	2.145	2.624	2.977	3.787	4.140
15	0.000	0.691	0.866	1.074	1.341	1.753	2.131	2.602	2.947	3.733	4.073
16	0.000	0.690	0.865	1.071	1.337	1.746	2.120	2.583	2.921	3.686	4.015
17	0.000	0.689	0.863	1.069	1.333	1.740	2.110	2.567	2.898	3.646	3.965
18	0.000	0.688	0.862	1.067	1.330	1.734	2.101	2.552	2.878	3.610	3.922
19	0.000	0.688	0.861	1.066	1.328	1.729	2.093	2.539	2.861	3.579	3.883
20	0.000	0.687	0.860	1.064	1.325	1.725	2.086	2.528	2.845	3.552	3.850
21	0.000	0.686	0.859	1.063	1.323	1.721	2.080	2.518	2.831	3.527	3.819
22	0.000	0.686	0.858	1.061	1.321	1.717	2.074	2.508	2.819	3.505	3.792
23	0.000	0.685	0.858	1.060	1.319	1.714	2.069	2.500	2.807	3.485	3.768
24	0.000	0.685	0.857	1.059	1.318	1.711	2.064	2.492	2.797	3.467	3.745
25	0.000	0.684	0.856	1.058	1.316	1.708	2.060	2.485	2.787	3.450	3.725
26	0.000	0.684	0.856	1.058	1.315	1.706	2.056	2.479	2.779	3.435	3.707
27	0.000	0.684	0.855	1.057	1.314	1.703	2.052	2.473	2.771	3.421	3.690
28	0.000	0.683	0.855	1.056	1.313	1.701	2.048	2.467	2.763	3.408	3.674
29	0.000	0.683	0.854	1.055	1.311	1.699	2.045	2.462	2.756	3.396	3.659
30	0.000	0.683	0.854	1.055	1.310	1.697	2.042	2.457	2.750	3.385	3.646
40	0.000	0.681	0.851	1.050	1.303	1.684	2.021	2.423	2.704	3.307	3.551
60	0.000	0.679	0.848	1.045	1.296	1.671	2.000	2.390	2.660	3.232	3.460
80	0.000	0.678	0.846	1.043	1.292	1.664	1.990	2.374	2.639	3.195	3.416
100	0.000	0.677	0.845	1.042	1.290	1.660	1.984	2.364	2.626	3.174	3.390
1000	0.000	0.675	0.842	1.037	1.282	1.646	1.962	2.330	2.581	3.098	3.300
z	0.000	0.674	0.842	1.036	1.282	1.645	1.960	2.326	2.576	3.090	3.291
	0%	50%	60%	70%	80%	90%	95%	98%	99%	99.8%	99.9%
	Confidence Level										

Figure 43: Students T-Table

VITA

Tanner Price

Candidate for the Degree of

Master of Science

Thesis: DESIGN AND EVALUATION OF A SMALL-SCALE PORTABLE HYBRID ROCKET ENGINE TEST STAND

Major Field: Mechanical and Aerospace Engineering

Biographical:

Education:

Completed the requirements for the Master of Science in Mechanical and Aerospace Engineering at Oklahoma State University, Stillwater, Oklahoma in May, 2023.

Completed the requirements for the Bachelor of Science in Mechanical Engineering at Oklahoma State University, Stillwater, Oklahoma in 2021.

Completed the requirements for the Bachelor of Science in Aerospace Engineering at Oklahoma State University, Stillwater, Oklahoma in 2021.

Professional Membership:

American Institute of Aeronautics and Astronautics